

---

# An Empirical Study of Assumptions in Bayesian Optimisation

---

**Alexander I. Cowen-Rivers\***  
Huawei Noah's Ark Lab, R&D London  
Technische Universität Darmstadt

**Wenlong Lyu\***  
Huawei Noah's Ark Lab

**Rasul Tutunov\***  
Huawei Noah's Ark Lab, R&D London

**Zhi Wang**  
Huawei Noah's Ark Lab

**Antoine Grosnit**  
Huawei Noah's Ark Lab, R&D London

**Ryan Rhys Griffiths**  
Huawei Noah's Ark Lab, R&D London  
University of Cambridge

**Hao Jianye**  
Huawei Noah's Ark Lab

**Jun Wang**  
Huawei Noah's Ark Lab, R&D London  
University College London

**Jan Peters**  
Technische Universität Darmstadt

**Haitham Bou Ammar**  
Huawei Noah's Ark Lab, R&D London  
University College London<sup>†</sup>

## Abstract

Inspired by the increasing desire to efficiently tune machine learning hyper-parameters, in this work we rigorously analyse conventional and non-conventional assumptions inherent to Bayesian optimisation. Across an extensive set of experiments we conclude that: 1) the majority of hyper-parameter tuning tasks exhibit heteroscedasticity and non-stationarity, 2) multi-objective acquisition ensembles with Pareto-front solutions significantly improve queried configurations, and 3) robust acquisition maximisation affords empirical advantages relative to its non-robust counterparts. We hope these findings may serve as guiding principles, both for practitioners and for further research in the field.

## 1 Introduction

Although achieving significant success in numerous applications [1, 2, 3, 4, 5], the performance of machine learning models chiefly depends on the correct setting of hyper-parameters. As models grow larger and more complex, efficient and autonomous hyper-parameter tuning algorithms become crucial determinants of performance. To this end, a variety of methods from black-box and multi-fidelity optimisation have been adopted [6, 7] with varying degrees of success. Techniques such as Bayesian optimisation (BO), for example, enable sample efficiency (in terms of black-box evaluations) at the expense of high computational demands, while “unguided” bandit-based approaches can fail to converge [8]. Identifying such failure modes, the authors in [8] built on [9] to propose a combination of

---

\*Equal contribution

<sup>†</sup>Honorary position.

bandits and BO that achieves the best of both worlds; fast convergence and computational scalability. Though impressive, such successes of BO and alternatives, conceal a set of restrictive modelling and acquisition function assumptions that are hindering the widespread adoption of BO. We begin by describing these assumptions.

**Modelling Assumptions:** Critical to BO performance is a set of data modelling assumptions that admit an effective probabilistic model of the true black-box objective (e.g., validation loss in hyper-parameter tuning tasks). This model should not only provide accurate point estimates, but should also maintain calibrated uncertainty estimates to guide exploration of the objective. Amongst many possible surrogates [10, 11], Gaussian processes [12] (GPs) are the default choice due to their flexibility and sample efficiency. Growing interest in applications of Bayesian optimisation has catalysed significant engineering feats enhancing the scalability and training efficiency of GP surrogates by exploiting graphical processing units [13, 14].

Similar to any other framework, the correct specification of a GP model is dictated by the data modelling assumptions imposed by the user. For instance, a homoscedastic GP suffers when asked to model data with heteroscedastic noise whilst stationary GPs fail to track non-stationary targets. Of course, the aforementioned shortcomings are not unnatural in real-world problems but arise precisely in tasks related to hyper-parameter tuning of machine learning algorithms as depicted in our tests in Section 3.2. Hence, even if one improves computational efficiency, commonly-made assumptions such as homoscedasticity and stationarity may easily hinder any tuning algorithm’s performance. Despite the importance of these assumptions in practice, GPs that presume homoscedasticity and stationarity are typically taken at face value and implemented as is.

**Acquisition Function & Optimiser Assumptions:** Modelling choices like those mentioned above are not unique to the fitting procedure but rather transcend to other pivotal steps of hyper-parameter tuners. Precisely, given a model that adheres to some (or all) assumptions mentioned above, the second step involves maximising an acquisition function to query novel input locations that are then evaluated. Hence, practitioners introduce additional constraints relating to the category of optimisation variables and the choice of acquisitions. When it comes to variable types, main-stream implementations [13, 14] assume continuous domains and employ first and second-order optimisers e.g., LBFGS [15] and ADAM [16] to determine queried points. Real-valued configurations cover but a subset of possible machine learning hyper-parameters rendering discrete types, like hidden layer size in deep networks, out of scope. Moreover, from the point of view of acquisition functions, libraries tend to presuppose that one unique acquisition performs best in a given task, limiting benefits that can arise from a combined solution as we demonstrate in Section 5.

**Contributions:** Having identified essential modelling choices in BO, our goal in this paper is to provide empirical insight into their affect on experimental performance with the aim of informing the community on best practices for hyper-parameter tuning. We wish for our findings to apply to a broad array of tasks and datasets, be attentive to the affect of random initialisation on algorithmic performance, and naturally, be reproducible. As such, we prefer to build on already established benchmark packages, especially those that enable fast and scalable evaluations sanctioning multi-seeding protocols. To that end, we undertake our evaluation in 2140 experiments from 108 real-world problems from the UCI repository [17], which also featured as a testbed in the NeurIPS 2020 black-box optimisation challenge [18]. Our empirical findings point towards the following conclusions:

1. Hyper-parameter tuning of machine learning tasks exhibit significant levels of heteroscedasticity and non-stationarity;
2. Applying input-warping and output transformation mitigates these affects giving rise to more well-behaved tuners with higher mean, and median performance across all 108 black-box functions under examination;
3. Individual acquisition functions tend to conflict in their solution (i.e., an optimum for one can be a bad point for the other and vice versa). Using a multi-objective formulation significantly improves performance;
4. Targeting robust formulations of acquisitions admit better tuners.

To further solidify our conclusions, we conducted additional ablation studies, realising a ranked order of importance in significant components. We found that output warping (conclusion 2), multi-objective acquisitions (conclusion 3) and input warping (conclusion 2) led to the most significant improvements followed by the robustness of acquisitions (conclusion 4).

## 2 Standard Design Choices in BO

As discussed earlier, the problem of hyper-parameter tuning can be framed as an instance of black-box optimisation:

$$\arg \max_{\mathbf{x} \in \mathcal{X}} f(\mathbf{x}), \quad (1)$$

with  $\mathbf{x}$  denoting a configuration choice,  $\mathcal{X}$  a (potentially) mixed design space, and  $f(\mathbf{x})$  a validation accuracy we wish to maximise.

In this paper, we focus on BO as a solution concept for black-box problems of the form depicted in Equation 1. BO considers a sequential decision approach to the global optimisation of a function  $f : \mathcal{X} \rightarrow \mathbb{R}$  over a bounded input domain  $\mathcal{X}$ . At each decision round,  $i$ , the algorithm selects a collection of  $q$  inputs  $\mathbf{x}_{1:q}^{(\text{new})} \in \mathcal{X}^q$  and observes values of the *black-box* function  $\mathbf{y}_{1:q}^{(\text{new})} = f(\mathbf{x}_{1:q}^{(\text{new})})$ . The goal is to rapidly approach the maximum  $\mathbf{x}^* = \arg \max_{\mathbf{x} \in \mathcal{X}} f(\mathbf{x})$ . Since both  $f(\cdot)$  and  $\mathbf{x}^*$  are unknown, solvers need to trade off exploitation and exploration during this search process.

To achieve this goal, BO algorithms operate in two steps. In the first, a Bayesian model is learned, while in the second an acquisition function determining new query locations is maximised. Next, we survey frequently-made assumptions in mainstream BO implementations and contemplate their implications on performance.

### 2.1 Modelling Assumptions

When black-boxes are real-valued, Gaussian process regression [19] are affective surrogates due to their flexibility and ability to maintain calibrated uncertainty estimates. In established implementations of BO, designers place GP priors on latent functions,  $f(\cdot)$ , which are fully specified through a mean function,  $m(\mathbf{x})$ , and a covariance function or kernel  $k_\theta(\mathbf{x}, \mathbf{x}')$  with  $\theta$  representing kernel hyper-parameters. The model specification is completed by defining a likelihood. Here, practitioners typically assume that observations  $y_l$  adhere to a Gaussian noise model such that  $y_l = f(\mathbf{x}_l) + \epsilon_l$  where  $\epsilon_l \sim \mathcal{N}(0, \sigma_{\text{noise}}^2)$ . This, in turn, generates a Gaussian likelihood of the form  $y_l | \mathbf{x}_l \sim \mathcal{N}(f_l, \sigma_{\text{noise}}^2)$  where we use  $f_l$  to denote  $f(\mathbf{x}_l)$  with  $f(\mathbf{x}) \sim \mathcal{GP}(m(\mathbf{x}), k_\theta(\mathbf{x}, \mathbf{x}'))$ . Additionally, a further design choice commonly made by practitioners is that the GP kernel is stationary, depending only on the norm between  $\mathbf{x}$  and  $\mathbf{x}'$ ,  $\|\mathbf{x} - \mathbf{x}'\|$ . From this exposition, we conclude two important modelling assumptions stated as *data stationarity* and *homoscedasticity of the noise distribution*. If the true latent process does not adhere to these assumptions, the resultant model will be a poor approximation to the black-box. Realising the potential empirical affects of these modelling choices, we identify the first two questions of this paper:

**Q.I.** Are parameter tuning tasks stationary?

**Q.II.** Are parameter tuning tasks homoscedastic?

In Section 3.2, we show that even the simplest among machine learning tasks pass tests of heteroscedasticity and non-stationarity.

### 2.2 Acquisitions & Optimisation Assumptions

Acquisition functions trade off exploration and exploitation by utilising statistics from the posterior  $p_\theta(f(\cdot) | \mathcal{D})$  with  $\mathcal{D}$  denoting data (parameter configurations as inputs and validation accuracy as outputs) collected so far. Under a GP surrogate, such a posterior is Gaussian itself. To simplify the exposition, we defer the exact equations to Appendix B.1 and just note that  $p(f(\mathbf{x}_{1:q}) | \mathcal{D}) = \mathcal{N}(\boldsymbol{\mu}_\theta(\mathbf{x}_{1:q}), \boldsymbol{\Sigma}_\theta(\mathbf{x}_{1:q}))$ . In this paper, we focus on three widely-used myopic acquisition functions which in a reparameterised form can be written as [20]:

**Expected improvement (EI):**

$$\alpha_{\text{EI}}^\theta(\mathbf{x}_{1:q} | \mathcal{D}) = \mathbb{E}_{\text{post.}} \left[ \max_{j \in 1:q} \{\text{ReLU}(f(\mathbf{x}_j) - f(\mathbf{x}^+))\} \right],$$

where the subscript post. is the predictive posterior of a GP [19],  $\mathbf{x}_j$  is the  $j^{\text{th}}$  vector of  $\mathbf{x}_{1:q}$ , and  $\mathbf{x}^+$  is the best performing input in the data so far.

Table 1: Hypothesis Testing for 108 tasks. We find that output transformations which tackle heteroscedasticity significantly improve GP modelling capabilities. Similarly, input transformations which tackle non-stationarity significantly improve GP modelling capabilities.

	Better	Sig. Better	Worse	Sig. Worse
Heteroscedasticity (Output Transform)	70 (65%)	58 (54%)	38 (35%)	25 (23%)
Non-Stationarity (Input Warping)	106 (98%)	79 (73%)	2 (2%)	0 (0%)

#### Probability of improvement (PI):

$$\alpha_{\text{PI}}^{\theta}(\mathbf{x}_{1:q}|\mathcal{D}) = \mathbb{E}_{\text{post.}} \left[ \max_{j \in 1:q} \{ \mathbb{1} \{ f(\mathbf{x}_j) - f(\mathbf{x}^+) \} \} \right],$$

where  $\mathbb{1} \{ \cdot \}$  is the left-continuous Heaviside step function.

#### Upper confidence bound (UCB):

$$\alpha_{\text{UCB}}^{\theta}(\mathbf{x}_j) = \mathbb{E}_{\text{post.}} \left[ \max_{j \in 1:q} \left\{ \mu_{\theta}(\mathbf{x}_j) + \sqrt{\beta\pi/2} |\gamma_{\theta}(\mathbf{x}_j)| \right\} \right],$$

where  $\mu_{\theta}(\mathbf{x}_j)$  is the posterior mean of the predictive distribution and  $\gamma_{\theta}(\mathbf{x}_j) = f(\mathbf{x}_j) - \mu_{\theta}(\mathbf{x}_j)$ .

When it comes to practicality, generic BO implementations make additional assumptions during the acquisition maximisation step. First, it is assumed that one of the aforementioned acquisitions works best for a specific task, and that the GP model is an accurate approximation to the black-box. However, when it comes to real-world applications, both of these assumptions are hard to validate; the best-performing acquisition is challenging to identify up-front and GP models can easily be misspecified. With this in mind, we identify a further question that we wish to answer:

#### Q.III. Can acquisition function solutions conflict in hyper-parameter tuning tasks?

In the next section, we affirm that acquisitions can conflict even on the simplest of machine learning tasks. Moreover, we show that a robust formulation to tackle misspecification of acquisition maximisation can improve overall performance (see Section 4.2.1).

### 3 Modelling Assumption Analysis

Before proceeding to potential improvements to BO, we now detail several analyses we conducted to answer the questions (Q.I., Q.II., and Q.III.) posed in the previous section. Our analyses indicates:

**A.I.** (Answer to **Q.I.**): Even simple machine learning tasks exhibit significant heteroscedasticity.

**A.II.** (Answer to **Q.II.**): Even simple machine learning tasks exhibit significant non-stationarity.

**A.III.** (Answer to **Q.III.**): Acquisition functions conflict in their optima, occasionally leading to opposing solutions. **Experimental Setting:** We create a wide range of hyper-parameter tasks (108) across a variety of classification and regression problems. We use nine models, (e.g. multi-layer perceptrons, support-vector machines) and six datasets (two regression and four classification) from the UCI repository, and two metrics per dataset such as negative log-likelihood or mean squared error. Each of the models possess tune-able hyper-parameters, e.g. the number of units of a neural network. The goal is to fit those hyper-parameters so as to maximise/minimise one of the metrics previously mentioned. Of course, such black-box values are stochastic with randomness originating from various sources, e.g., train-test splits to compute losses and random seeds. Experimentation was facilitated by the Bayesmark<sup>3</sup> packaged. Full hyper-parameter search spaces defined over Table 2 and Table 3 in the Appendix<sup>4</sup>.

#### 3.1 Answer A.I.: Simple Tasks are Non-Stationary

To provide answers to **Q.I.**, we run tests to *gauge non-stationarity affecting BO performance*. To assess the impact of the extent of non-stationarity on BO performance, we conduct probabilistic

<sup>3</sup><https://github.com/uber/bayesmark>

<sup>4</sup>It is these search spaces used by the random search baseline.

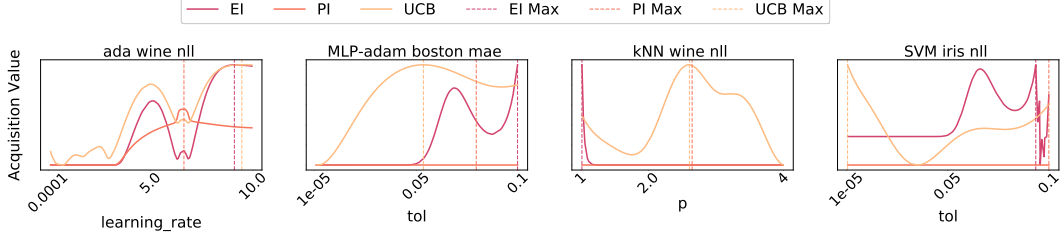


Figure 1: Examples depicting conflicting acquisitions across varying datasets (Wine, Boston Housing, and Iris) and models (AdaBoost, Multi-Layer perceptron, K-Nearest neighbours, and support vector machines).

regression experiments to gauge the predictive performance of a stationary GP on the hyper-parameter tuning tasks with and without input warping which corrects for non-stationarity. We posit that the quality of the surrogate model is a good proxy for BO performance. We first run a two-sided paired t-test for each of the 108 tasks where the null hypothesis is that the application of the input warping yields no difference in the log probability metric. Table 1 significance tests show that in 106/108 tasks, the log probability metric is better when input warping is applied. In 79/108 tasks, the gain is significant at the 95% level of confidence (p-value < 0.025). We thus conclude that non-stationarity affects BO performance due to having a significant affect on GP regression’s log probability metric.

### 3.2 Answers A.II.: Simple Tasks are Heteroscedastic

To provide answers to **Q.II.**, we run tests to *gauge heteroscedasticity affecting BO performance*. We perform an analogous hypothesis test as in subsection 3.1, assessing a vanilla GP’s performance with and without output transforms (Box-Cox/ Yeo-Johnson). We run a two-sided paired t-test for each of the 108 tasks where the null hypothesis is that the application of the output transform yields no difference in the log probability metric. Table 1 significance tests show in 70/108 tasks, the log probability metric is better when output transforms are applied. In 58/108 tasks, the gain is significant at the 95% level of confidence (p-value < 0.025). We thus conclude that heteroscedasticity affects BO performance due to having a significant affect on GP regression’s log probability metric.

Secondly, to *gauge heteroscedasticity in the underlying data*, we use Fligner and Killeen [21] and Levene [22] tests. It was shown in [23] that both these tests are reliable in terms of robustness to departures from normality [24]. Both test the null hypothesis that the underlying black-box function (e.g., validation accuracy (**hyper-parameter**<sub>*i*</sub>)) is homoscedastic. In all 108 tests, we see a p-value significantly lower than 0.05 in 72 tasks using Levene’s test, and in 73 tasks using Fligner and Killeen. Such results (shown in detail in Appendix D) imply that at least 66% of the experimental tasks exhibit heteroscedastic behaviour.

### 3.3 Answer A.III.: A No Clear Winner

It has been observed before that multi objectives can conflict [25]. To answer **Q.III.** of whether acquisition functions can conflict in their solutions, we collect 128 samples from each task by evaluating various hyper-parameter configurations across different metrics. We then gather a dataset  $\mathcal{D} = \{\mathbf{hyper-param}_i, y_i\}_{i=1}^{32}$ , where **hyper-param**<sub>*i*</sub> is a vector whose dimensionality depends on the number of hyper-parameters in a given model, and  $y_i$  corresponds to an evaluation metric, e.g., mean squared error (**hyper-param**<sub>*i*</sub>). We then fit a GP surrogate model and consider each of the three acquisitions from Section 2.2. As its difficult to graphically depict an acquisition conflict in more than 2 dimensions, we analysed a simplified 2D scenario. From Figure 1, we realise that even in the simplest 2D case, many examples of conflicting acquisitions exist. Thus, its probable that in higher dimension space this behaviour can similarly occur. The full set of results can be found in the Appendix E.

## 4 Optimising Bayesian Optimisation

Now, we elaborate on more general design choices that prove empirically effective. Some of the forthcoming remedies have been proposed elsewhere in settings beyond BO, while acquisition function robustness is unique to this work.

### 4.1 Tackling Heteroscedasticity and Non-Stationarity

To enable flexible modelling solutions capable of handling heteroscedasticity and non-stationarity, we apply ideas from the warped GP literature [26] where output transformations allow for more complex noise processes. We found that the Box-Cox [27] and Yeo-Johnson [28] output transformations and a Kumaraswamy [29] input warping offered a balance of simplicity in implementation and empirical performance. In fact, in our ablation study (Section 5), we demonstrate that the addition of these two modelling components resulted in large performance gains.

**Output Transformation for Heteroscedasticity:** We consider the Box-Cox transformation typically used to map non-Gaussian data closer to “Gaussianity”. The class of transforms depend on a tuneable parameter  $\zeta$  and apply the following map to each of the labels:  $T_\zeta(y_l) = y_l^\zeta - 1/\zeta$  for  $\zeta \neq 0$  and  $T_\zeta(y_l) = \log y_l$  if  $\zeta = 0$ , where in our case  $y_l$  denotes a validation accuracy of the  $l^{\text{th}}$  hyper-parameter configuration. Of course,  $\zeta$  has to be fit based on the observed data such that the distribution of the transformed labels closely resembles a Gaussian. This is achieved by minimising the negative of the Box-Cox likelihood function:

$$\log \left[ \sum_{l=1}^n \frac{(T_\zeta(y_l) - \bar{T}_\zeta(\mathbf{y}))^2}{n} \right]^{\frac{n}{2}} + \sum_{l=1}^n \log [T_\zeta(y_l)]^{(1-\zeta)},$$

where  $n$  is the number of datapoints and  $\bar{T}_\zeta(\mathbf{y})$  is the sample mean of the transformed labels. Of course, Box-Cox transforms only considers strictly positive (or strictly negative) labels  $y_l$ . To handle a more general setting, we also make use of the Yeo-Johnson transform [28]. Due to space constraints we defer the details to Appendix B.2.

**Input Transformations for Non-Stationarity:** Having dealt with heteroscedasticity, now we shift our attention to tackle data non-stationarity. As a general solution concept, we consider input warping see [30]. In our implementation, we relied on a Kumaraswamy input warping, which executes the following for each of the input dimensions:

$$[\text{Kumaraswamy}_\gamma(\mathbf{x}_l)]_k = 1 - (1 - [\mathbf{x}_l]_k^{a_k})^{b_k} \quad \forall k \in [1 : d],$$

with  $d$  being the dimensionality of the decision variable (e.g., number of free hyper-parameters),  $a_k$  and  $b_k$  are tuneable warping parameters for each of the dimensions, and  $\gamma$  is a vector concatenating all free parameters, i.e.,  $\gamma = [a_{1:d}, b_{1:d}]^\top$ . Of course,  $\gamma$  is fit based on observed data. Similar to [14], we consider  $\gamma$  as part parameters of the marginal likelihood that we optimise while fitting our GP.

**All Modelling Improvements Together:** Combining the above considerations of heteroscedasticity and non-stationarity leads us to an improved GP model with more flexible capabilities. The implementation of such a model is relatively simple and involves maximising a new marginal that can be written as:

$$\max_{\boldsymbol{\theta}, \gamma} - \frac{1}{2} \mathbf{T}_{\zeta^*}(\mathbf{y})^\top (\mathbf{K}_{\boldsymbol{\theta}}^\gamma + \sigma_{\text{noise}}^2 \mathbf{I})^{-1} \mathbf{T}_{\zeta^*}(\mathbf{y}) - \frac{1}{2} |\mathbf{K}_{\boldsymbol{\theta}}^\gamma + \sigma_{\text{noise}}^2 \mathbf{I}| - \text{const},$$

where  $\boldsymbol{\theta}$  are GP hyper-parameters,  $\gamma$  corresponds to non-stationary transforms, and  $\zeta^*$  denotes the solution to a Box-Cox likelihood objective. It is worth noting that we used Box-Cox as a running example but as mentioned previously we interchange Box-Cox with Yeo-Johnson transforms based on the properties of the label  $y_l$ . Moreover, we used  $\mathbf{K}_{\boldsymbol{\theta}}^\gamma \in \mathbb{R}^{n \times n}$  to represent a matrix such that each entry depends on both  $\boldsymbol{\theta}$  and  $\gamma$ , where  $k_{\boldsymbol{\theta}}^\gamma(\mathbf{x}, \mathbf{x}') = k_{\boldsymbol{\theta}}(\text{Kumaraswamy}_\gamma(\mathbf{x}), \text{Kumaraswamy}_\gamma(\mathbf{x}'))$ .

### 4.2 Tackling Acquisition Conflict & Robustness

Having proposed modifications to the modelling process of BO, we now concentrate on the acquisition maximisation step. In particular, we handle two problems, one related to the assumption of a perfect GP surrogate, with the second centred around conflicting acquisitions.

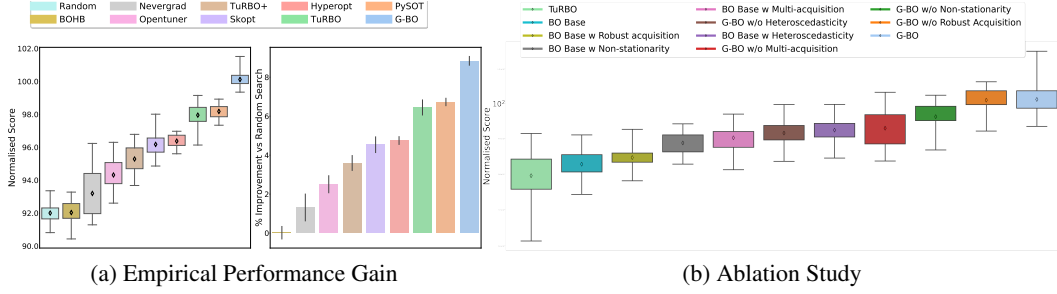


Figure 2: Analysis of the results on 108 tuning tasks. (a-Left) Normalised score comparison demonstrating that G-BO (i.e., BO with improvements from Section 4) outperforms others. (a-Right) Empirical gain demonstrating that G-BO can arrive at 8% improvement compared to random. (b-Left) Ablation study reflecting the importance of each component by taking one component out. (b-Right) Ablation study reflecting the importance of each component by adding one component. We see comparative performance to TuRBO with all significant components removed from G-BO, which we named BO Base. This further confirms the performance of G-BO is due to the revised assumptions.

#### 4.2.1 A Robust Acquisition Objective

As mentioned in Section 2.2, the acquisition maximisation step assumes that adequate surrogates are readily available. Especially during early rounds of training, such a property is hard to validate as data is scarce leading to (sometimes) severe model misspecification that hurts performance. One way to tackle such a problem is to assume a robust formulation [31, 32] that attempts to find the best performing query location under the worst-case GP model, i.e., solving  $\max_{\mathbf{x}} \min_{\boldsymbol{\theta}} \alpha^{\boldsymbol{\theta}}(\mathbf{x}|\mathcal{D})$ . Granted such a formulation allows for a solution  $\mathbf{x}^*$  that is robust to worst-case misspecification in  $\boldsymbol{\theta}$ , having a max min acquisition is troubling for several reasons. From a conceptual perspective max min formulations are known to lead to very conservative solutions if not correctly constrained or regularised since the optimiser possesses the power to impair the GP fit while updating  $\boldsymbol{\theta}$ <sup>5</sup>. From an implementation perspective, one faces two further issues. First, no global convergence guarantees are known for the non-convex non-concave case that we face [34], and second, ensuring gradients can propagate through the computation graph restrict surrogates and acquisition functions to be within the same programming framework.

To avoid worst-case solutions and enable independence between acquisition functions and surrogate models, we borrow ideas from domain randomisation [35] and consider an expected formulation instead:  $\max_{\mathbf{x}} \alpha_{\text{rob}}(\cdot) \equiv \max_{\mathbf{x}} \mathbb{E}_{\epsilon \sim \mathcal{N}(\mathbf{0}, \sigma_{\epsilon}^2 \mathbf{I})} [\alpha^{\boldsymbol{\theta} + \epsilon}(\mathbf{x}|\mathcal{D})]$ . Importantly, this problem seeks to find new query locations that perform well on average over a distribution of surrogate models rather than assuming a perfect surrogate.

Though appealing, our formulation still assumes access to the GP’s hyper-parameters, complicating implementation and restricting models and optimisers to the same programming paradigm. We wish to enable robustness by only having access to the GP’s mean and variance predictions for simplicity. Fortunately, we are able to show that upon a simple acquisition perturbation one can approximate the above  $\alpha_{\text{rob}}(\cdot)$ . Namely, we prove (see Appendix B) that if  $\bar{\alpha}^{\boldsymbol{\theta}}(\mathbf{x}|\mathcal{D}) = \alpha^{\boldsymbol{\theta}}(\mathbf{x}|\mathcal{D}) + \eta\sigma_n$  with  $\eta \sim \mathcal{N}(0, 1)$ , then upon further technical details<sup>6</sup> we have (with high probability):

$$|\bar{\alpha}^{\boldsymbol{\theta}}(\mathbf{x}|\mathcal{D}) - \mathbb{E}_{\epsilon \sim \mathcal{N}(\mathbf{0}, \sigma_{\epsilon}^2 \mathbf{I})} [\alpha^{\boldsymbol{\theta} + \epsilon}(\mathbf{x}|\mathcal{D})]| \leq \rho,$$

for any arbitrary  $\rho \in (0, 1)$ .

The bound above enables uncomplicated yet effective, robust implementations. For instance, if we would like to “robustify” a UCB acquisition, we add  $\eta\sigma_n$  to the posterior’s mean and follow standard UCB onwards.

<sup>5</sup>Of course, one can argue augmenting the objective with a constraint such that  $\boldsymbol{\theta}$  updates remain close to  $\boldsymbol{\theta}^*$  of the marginal. The value by which such proximity needs to be enforced remains unclear in robust literature to date [31, 33].

<sup>6</sup>We would like to mention that though a gradient-based algorithm remains intact upon the addition of  $\eta\sigma_n$ , in our formulation we use an evolutionary method which utilises acquisition function values. Consequently, the path followed by the optimiser will be altered based on  $\eta$  samples leading to more robust probes.

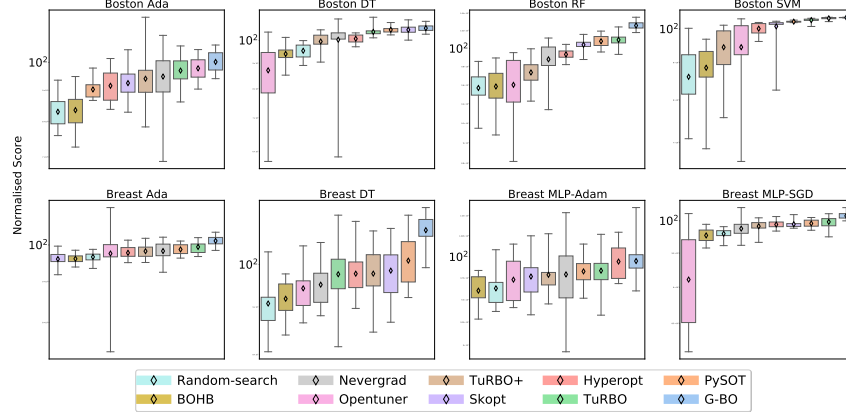


Figure 3: G-BO against all baselines on 16x8 suggestions. Each experiment repeated with 20 random seeds. We averaged each seed over both metrics in all 108 tasks to examine a reduced number of 54 distinct black-box functions. G-BO achieves the highest normalised mean score in optimising 68.5% of the black-box functions. We highlight 8 of the 54 tasks above, and show the remaining in the Appendix.

#### 4.2.2 Multi-Objective Acquisitions

As a final component of our general framework, we propose the usage of multi-objective acquisitions and seek a Pareto-front solution concept. This formulation enables a form of “hedging” between different acquisitions such that any other acquisition does not dominate the solution, thus representing the best solution trade-off [36]. Formally, we solve:

$$\max_{\mathbf{x}} (\bar{\alpha}_{\text{EI}}^{\theta}(\mathbf{x}|\mathcal{D}), \bar{\alpha}_{\text{PI}}^{\theta}(\mathbf{x}|\mathcal{D}), \bar{\alpha}_{\text{UCB}}^{\theta}(\mathbf{x}|\mathcal{D})) , \quad (2)$$

where  $\bar{\alpha}_{\text{type}}^{\theta}(\mathbf{x}|\mathcal{D})$  is a robust acquisition as introduced in the previous section and  $\text{type} \in \{\text{EI}, \text{PI}, \text{UCB}\}$ . We also note that our formulation is meant to reflect the fact of using a robust objective value of  $\bar{\alpha}^{\theta}(\mathbf{x}|\mathcal{D}) = \alpha^{\theta}(\mathbf{x}|\mathcal{D}) + \eta_k \sigma_n$  with  $\eta_k$  being a sample from  $\mathcal{N}(0, 1)$  at each iteration of the evolutionary solver.

Although solving the problem in Equation 2 is a formidable challenge, we note the existence of many mature multi-objective optimisation algorithms. These range from first-order [37] to zero-order [38, 39] and evolutionary methods [40, 41]. Due to the discrete nature of hyper-parameters in machine learning tasks, we advocate using evolutionary solvers that naturally handle categorical and integer-valued variables. In our experiments, we employ the non-dominated sorting genetic algorithm II (NSGA-II) that allows for mixed variable crossover and mutation to optimise real and integer input types [41]. Importantly, an available stable implementation of NSGA-II along with other solvers can be found in the latest release of Pymoo [42]. Alternatively, one could use the GP Hedge acquisition which select between acquisitions and is used in Dragonfly [43], [44] and SkOpt. In experiments however, we found this to work poorly against individual acquisitions.

## 5 Performance Experimentation

In this section, we continue our empirical evaluation and validate gains (if any) that arise from the improvements proposed in section 4. The experimental setup is as described in section 3. To measure performance, we use the normalised task score<sup>7</sup> (as detailed in Appendix 14) to compare across tasks. We run experiments on either 16 iterations of 8 suggestions (16x8) or 100 iterations of 1 suggestion (100x1). With each experiment repeated for 20 random seeds.

We also experiment with a wider range of solvers that either rely on BO-strategies or follow zero-order techniques such as differential evolution or particle swarms. These include SkOpt [45]<sup>8</sup>

<sup>7</sup>Note, we don’t report suggestion time per algorithm as this was under 20 seconds per suggestion batch.

<sup>8</sup><https://github.com/scikit-optimize/scikit-optimize>



pySOT<sup>9</sup> a parallel global optimisation package [46], HyperOpt [47]<sup>10</sup>, OpenTuner<sup>11</sup> a package allowing for ensemble of methods [48], NeverGrad [49]<sup>12</sup> a gradient-free optimisation toolbox (with One Plus One optimiser), BOHB [8]<sup>13</sup> and Dragonfly [43]<sup>14</sup>. Additionally, we carried our modelling improvements to TuRBO<sup>15</sup>, augmenting the standard GP with remedies from Section 4 effectively producing a new baseline that we entitle TuRBO+. Finally, we introduce Gauged Bayesian Optimisation G-B0, in which we construct an optimiser with improvements introduced in section 4. Figure 2 demonstrates gains from adopting the general G-B0 framework. In Figure 2 (a), we compare G-B0 against other baselines and report up to 8% performance gain compared to a random search strategy. It is also worth noting that TuRBO+ tended to under-perform<sup>16</sup>, achieving ca. 4% improvement relative to random search. We believe such a result is related to the interplay between our approach’s capabilities to address heteroscedasticity and non-stationarity as well as the size of the trust-regions; an interesting avenue that we plan to explore in future work. We also elaborate further results in Figure 3 across multiple datasets and models. Overall, G-B0 achieves highest normalised mean scores in 74 out of 108 datasets. Further results on all tasks can be found in Appendix C.3.

**Comparison to asynchronous BO algorithms:** Dragonfly and BOHB are asynchronous algorithms which perform one suggestion per request. In order to impartially evaluate their suggestion function, we run them against the top 3 batch Bayesian optimisation algorithms on 100x1 suggestions. Figure 4 shows significant under-performance by Dragonfly and BOHB vs all other BO methods. Lastly, we observe G-B0 performing dominant.

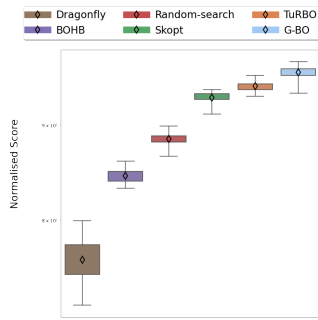


Figure 4: 100x1 on 108 tasks.

**Ablation Results:** To better understand each addition’s contribution of G-B0, we conducted two ablation studies by first removing each component and testing the remaining. Specifically, we removed either heteroscedasticity (G-B0 w/o heteroscedasticity), non-stationarity, robustness, and the multi-acquisition components, ran BO with the remaining ingredients, and reported average normalised scores in Figure 2. Secondly, we perform another ablation by first starting with Base BO (G-B0 w/o all four components), then evaluated Base BO with at most one component included. Results from both ablations are shown in Figure 2. Figure 2 reveals the following significance ordering; heteroscedasticity, multi-acquisition, non-stationarity and robustness.

## 6 Related Work

We introduce work on the following topics relating to modelling, acquisition and optimisers in Bayesian optimisation:

**Heteroscedasticity with output transforms:** Among various approaches to handling heteroscedasticity [50, 51, 52, 53, 54], transforming the output variables is a straightforward option giving rise to warped Gaussian processes [26]. More recently, output transformations have been extended to compositions of elementary functions [55] and normalising flows [56, 57]. Output transformations have not featured prominently in the Bayesian optimisation literature, perhaps due to the commonly-held opinion that warped GPs require more data relative to standard GPs in order to function as affective surrogates [58]. Rather than introducing additional hyper-parameters to the GP, we enable efficient output warping through methods that only require pre-training.

**Non-stationarity with input warpings:** Many surrogate models with input warpings exist for optimising non-stationary black-box objectives [59, 60, 61] and have enjoyed particular success in hyperparameter tuning where the natural scale of parameters is often logarithmic. Traditionally, a Beta cumulative distribution function is used. In this paper, we adopt the Kumaraswamy warping

<sup>9</sup><https://github.com/dme65/pySOT>

<sup>10</sup><https://github.com/hyperopt/hyperopt>

<sup>11</sup><https://github.com/jansel/opentuner>

<sup>12</sup><https://github.com/facebookresearch/nevergrad>

<sup>13</sup><https://github.com/automl/HpBandSter>

<sup>14</sup><https://github.com/dragonfly/dragonfly>

<sup>15</sup>[https://github.com/rdturnermtl/bbo\\_challenge\\_starter\\_kit/](https://github.com/rdturnermtl/bbo_challenge_starter_kit/)

<sup>16</sup>We believe this due to the trust region not being modelled correctly with input warping.

which is another instance of the generalised Beta class of distributions which we have observed to achieve superior performance to [59]; confirming results reported in [14].

**Multi-objective acquisition ensembles:** Multi-objective acquisition ensembles were first proposed in [36] and are closely related to portfolios of acquisition functions [14, 25, 62]. In this form, the optimisation problem involves at least two conflicting and expensive black-box objectives and as such, solutions are located along the Pareto-efficient frontier. The multi-objective acquisition ensemble employs these ideas to find a Pareto-efficient solution amongst multiple acquisition functions. Although we utilised the multi-objective acquisition ensemble, we note that our framework is solver agnostic in so far as any multi-objective optimiser [63] may be applied.

**Robustness of Acquisitions:** Methods achieving robustness with respect to either surrogates [64] or the optimisation process [65, 66] have been previously proposed. Most relevant to our setting, is the approach of [65] that introduces robustness to BO by solving a max min objective to determine optimal input perturbations. Their method, however, relies on gradient ascent-descent-type algorithms that require real-valued variables and are not guaranteed to converge in the general non-convex, non-concave setting [34]. On the other hand, our solution possesses two advantages: 1) simplicity of implementation as we merely require random perturbations of acquisition functions to guarantee robustness, and 2) support for mixed variable solutions through the use of evolutionary solvers.

## 7 Conclusion & Future Work

In this paper, we presented an in-depth empirical study of Bayesian optimisation. We demonstrated that even the simplest among machine learning problems can exhibit heteroscedasticity and non-stationarity. We also reflected on the affects of misspecified models and conflicting acquisition functions. We augmented BO algorithms with various enhancements and revealed that with a revised set of assumptions BO can in fact act as a competitive baseline in hyper-parameter tuning. We hope this paper’s findings can guide the community when employing BO in practice.

## References

- [1] Jesús Bobadilla, Fernando Ortega, Antonio Hernando, and Abraham Gutiérrez. Recommender systems survey. *Knowledge-Based Systems*, 46:109–132, 2013.
- [2] Geert Litjens, Thijs Kooi, Babak Ehteshami Bejnordi, Arnaud Arindra Adiyoso Setio, Francesco Ciompi, Mohsen Ghafoorian, Jeroen AWM Van Der Laak, Bram Van Ginneken, and Clara I Sánchez. A survey on deep learning in medical image analysis. *Medical Image Analysis*, 42:60–88, 2017.
- [3] Meherwar Fatima and M. Pasha. Survey of machine learning algorithms for disease diagnostic. *Journal of Intelligent Learning Systems and Applications*, 09:1–16, 2017.
- [4] Kirthivasan Kandasamy, Willie Neiswanger, Jeff Schneider, Barnabás Póczos, and Eric P Xing. Neural architecture search with Bayesian optimisation and optimal transport. In *Proceedings of the 32nd International Conference on Neural Information Processing Systems*, pages 2020–2029, 2018.
- [5] Alexander I Cowen-Rivers, Daniel Palenicek, Vincent Moens, Mohammed Abdullah, Aivar Sootla, Jun Wang, and Haitham Bou-Ammar. SAMBA: Safe model-based & active reinforcement learning. *arXiv preprint arXiv:2006.09436*, 2020.
- [6] Kirthivasan Kandasamy, Gautam Dasarathy, Jeff Schneider, and Barnabás Póczos. Multi-fidelity Bayesian optimisation with continuous approximations. In *International Conference on Machine Learning*, pages 1799–1808, 2017.
- [7] Rajat Sen, Kirthivasan Kandasamy, and Sanjay Shakkottai. Multi-fidelity black-box optimization with hierarchical partitions. In *International Conference on Machine Learning*, pages 4538–4547. PMLR, 2018.
- [8] Stefan Falkner, Aaron Klein, and Frank Hutter. Bohb: Robust and efficient hyperparameter optimization at scale. In *International Conference on Machine Learning*, pages 1437–1446. PMLR, 2018.

- [9] Lisha Li, Kevin Jamieson, Giulia DeSalvo, Afshin Rostamizadeh, and Ameet Talwalkar. Hyperband: A novel bandit-based approach to hyperparameter optimization. *The Journal of Machine Learning Research*, 18(1):6765–6816, 2017.
- [10] Jost Tobias Springenberg, Aaron Klein, Stefan Falkner, and Frank Hutter. Bayesian optimization with robust Bayesian neural networks. In *Advances in Neural Information Processing Systems*, pages 4134–4142, 2016.
- [11] Frank Hutter, Holger H Hoos, and Kevin Leyton-Brown. Sequential model-based optimization for general algorithm configuration. In *International Conference on Learning and Intelligent Optimization*, pages 507–523. Springer, 2011.
- [12] Christopher KI Williams and Carl Edward Rasmussen. Gaussian processes for regression. 1996.
- [13] Nicolas Knudde, Joachim van der Herten, Tom Dhaene, and Ivo Couckuyt. GpflowOpt: a Bayesian optimization library using TensorFlow. In *Neural Information Processing Systems 2017 Workshop on Bayesian Optimization*, 2017.
- [14] Maximilian Balandat, Brian Karrer, Daniel Jiang, Samuel Daulton, Ben Letham, Andrew G Wilson, and Eytan Bakshy. BoTorch: A framework for efficient Monte-Carlo Bayesian optimization. *Advances in Neural Information Processing Systems*, 33, 2020.
- [15] D. C. Liu and J. Nocedal. On the limited memory BFGS method for large scale optimization. *Math. Programming*, 45(3):503–528, 1989.
- [16] Diederik P. Kingma and Jimmy Ba. Adam: A method for stochastic optimization. In Yoshua Bengio and Yann LeCun, editors, *3rd International Conference on Learning Representations, ICLR 2015, San Diego, CA, USA, May 7-9, 2015, Conference Track Proceedings*, 2015.
- [17] Dheeru Dua and Casey Graff. UCI machine learning repository, 2017.
- [18] Ryan Turner, David Eriksson, Michael McCourt, Juha Kiili, Eero Laaksonen, Zhen Xu, and Isabelle Guyon. Bayesian optimization is superior to random search for machine learning hyperparameter tuning: Analysis of the black-box optimization challenge 2020. *arXiv preprint arXiv:2104.10201*, 2021.
- [19] Carl Edward Rasmussen and Christopher KI Williams. *Gaussian Processes for Machine Learning*, volume 2. MIT press Cambridge, MA, 2006.
- [20] Ashia C Wilson, Rebecca Roelofs, Mitchell Stern, Nathan Srebro, and Benjamin Recht. The marginal value of adaptive gradient methods in machine learning. In *Proceedings of the 31st International Conference on Neural Information Processing Systems*, pages 4151–4161, 2017.
- [21] Michael A Fligner and Timothy J Killeen. Distribution-free two-sample tests for scale. *Journal of the American Statistical Association*, 71(353):210–213, 1976.
- [22] Howard Levene. Contributions to probability and statistics. *Essays in Honor of Harold Hotelling*, pages 278–292, 1960.
- [23] William J Conover, Mark E Johnson, and Myrle M Johnson. A comparative study of tests for homogeneity of variances, with applications to the outer continental shelf bidding data. *Technometrics*, 23(4):351–361, 1981.
- [24] Chanseok Park and Bruce G Lindsay. Robust scale estimation and hypothesis testing based on quadratic inference function. Technical report, Center for Likelihood Studies, Department of Statistics, The Pennsylvania State University, 1999.
- [25] Bobak Shahriari, Ziyu Wang, Matthew W Hoffman, Alexandre Bouchard-Côté, and Nando de Freitas. An entropy search portfolio for Bayesian optimization. *arXiv preprint arXiv:1406.4625*, 2014.
- [26] Edward Snelson, Carl Edward Rasmussen, and Zoubin Ghahramani. Warped Gaussian processes. *Advances in Neural Information Processing Systems*, 16:337–344, 2004.

- [27] George EP Box and David R Cox. An analysis of transformations. *Journal of the Royal Statistical Society: Series B (Methodological)*, 26(2):211–243, 1964.
- [28] In-Kwon Yeo and Richard A Johnson. A new family of power transformations to improve normality or symmetry. *Biometrika*, 87(4):954–959, 2000.
- [29] Ponnambalam Kumaraswamy. A generalized probability density function for double-bounded random processes. *Journal of Hydrology*, 46(1-2):79–88, 1980.
- [30] Jasper Snoek, Hugo Larochelle, and Ryan P Adams. Practical Bayesian optimization of machine learning algorithms. In *Advances in Neural Information Processing Systems*, pages 2951–2959, 2012.
- [31] Johannes Kirschner, Ilija Bogunovic, Stefanie Jegelka, and Andreas Krause. Distributionally robust Bayesian optimization. In *International Conference on Artificial Intelligence and Statistics*, pages 2174–2184, 2020.
- [32] Aaron Klein, Stefan Falkner, Numair Mansur, and Frank Hutter. RoBo: A flexible and robust Bayesian optimization framework in Python. In *In Neural Information Processing Systems 2017 Workshop on Bayesian Optimization*, 2017.
- [33] Mohammed Amin Abdullah, Hang Ren, Haitham Bou Ammar, Vladimir Milenkovic, Rui Luo, Mingtian Zhang, and Jun Wang. Wasserstein robust reinforcement learning. *arXiv preprint arXiv:1907.13196*, 2019.
- [34] Tianyi Lin, Chi Jin, and Michael Jordan. On gradient descent ascent for nonconvex-concave minimax problems. In *International Conference on Machine Learning*, pages 6083–6093, 2020.
- [35] Josh Tobin, Rachel Fong, Alex Ray, Jonas Schneider, Wojciech Zaremba, and Pieter Abbeel. Domain randomization for transferring deep neural networks from simulation to the real world. In *2017 IEEE/RSJ International Conference on Intelligent Robots and Systems (IROS)*, pages 23–30. IEEE, 2017.
- [36] Wenlong Lyu, Fan Yang, Changhao Yan, Dian Zhou, and Xuan Zeng. Batch Bayesian optimization via multi-objective acquisition ensemble for automated analog circuit design. In *International Conference on Machine Learning*, pages 3306–3314, 2018.
- [37] Diederik P. Kingma and Max Welling. Auto-encoding variational Bayes. In Yoshua Bengio and Yann LeCun, editors, *2nd International Conference on Learning Representations, ICLR 2014, Banff, AB, Canada, April 14-16, 2014, Conference Track Proceedings*, 2014.
- [38] Ilya Loshchilov and Frank Hutter. CMA-ES for hyperparameter optimization of deep neural networks. *arXiv preprint arXiv:1604.07269*, 2016.
- [39] Victor Gabillon, Rasul Tutunov, Michal Valko, and Haitham Bou-Ammar. Derivative-free & order-robust optimisation. In *Proceedings of the Twenty Third International Conference on Artificial Intelligence and Statistics*, volume 108, pages 2293–2303, 2020.
- [40] Nikolaus Hansen. The CMA evolution strategy: A tutorial. *arXiv preprint arXiv:1604.00772*, 2016.
- [41] Kalyanmoy Deb, Amrit Pratap, Sameer Agarwal, and TAMT Meyarivan. A fast and elitist multiobjective genetic algorithm: NSGA-II. *IEEE Transactions on Evolutionary Computation*, 6(2):182–197, 2002.
- [42] J. Blank and K. Deb. Pymoo: Multi-objective optimization in Python. *IEEE Access*, 8:89497–89509, 2020.
- [43] Kirthevasan Kandasamy, Karun Raju Vysyaraju, Willie Neiswanger, Biswajit Paria, Christopher R. Collins, Jeff Schneider, Barnabas Poczos, and Eric P. Xing. Tuning hyperparameters without grad students: Scalable and robust bayesian optimisation with dragonfly. *Journal of Machine Learning Research*, 21(81):1–27, 2020.
- [44] Matthew D Hoffman, Eric Brochu, and Nando de Freitas. Portfolio allocation for bayesian optimization. In *UAI*, pages 327–336. Citeseer, 2011.

- [45] F. Pedregosa, G. Varoquaux, A. Gramfort, V. Michel, B. Thirion, O. Grisel, M. Blondel, P. Prettenhofer, R. Weiss, V. Dubourg, J. Vanderplas, A. Passos, D. Cournapeau, M. Brucher, M. Perrot, and E. Duchesnay. Scikit-learn: Machine learning in Python. *Journal of Machine Learning Research*, 12:2825–2830, 2011.
- [46] David Eriksson, David Bindel, and Christine A Shoemaker. pySOT and POAP: An event-driven asynchronous framework for surrogate optimization. *arXiv preprint arXiv:1908.00420*, 2019.
- [47] James Bergstra, Brent Komer, Chris Eliasmith, Dan Yamins, and David D Cox. Hyperopt: a Python library for model selection and hyperparameter optimization. *Computational Science & Discovery*, 8(1):014008, 2015.
- [48] Jason Ansel, Shoaib Kamil, Kalyan Veeramachaneni, Jonathan Ragan-Kelley, Jeffrey Bosboom, Una-May O’Reilly, and Saman Amarasinghe. Opentuner: An extensible framework for program autotuning. In *Proceedings of the 23rd International Conference on Parallel Architectures and Compilation*, pages 303–316, 2014.
- [49] J. Rapin and O. Teytaud. Nevergrad - A gradient-free optimization platform. <https://GitHub.com/FacebookResearch/Nevergrad>, 2018.
- [50] Kristian Kersting, Christian Plagemann, Patrick Pfaff, and Wolfram Burgard. Most likely heteroscedastic Gaussian process regression. In *Proceedings of the 24th International Conference on Machine Learning*, pages 393–400, 2007.
- [51] Miguel Lázaro-Gredilla and Michalis K Titsias. Variational heteroscedastic Gaussian process regression. In *Proceedings of the 28th International Conference on International Conference on Machine Learning*, pages 841–848, 2011.
- [52] Scott R Kuindersma, Roderic A Grupen, and Andrew G Barto. Variable risk control via stochastic optimization. *The International Journal of Robotics Research*, 32(7):806–825, 2013.
- [53] Roberto Calandra. *Bayesian modeling for optimization and control in robotics*. PhD thesis, Darmstadt, Technische Universität, 2017.
- [54] Ryan-Rhys Griffiths, Alexander A. Aldrick, Miguel Garcia-Ortegon, Vidhi R. Lalchand, and Alpha A. Lee. Achieving robustness to aleatoric uncertainty with heteroscedastic Bayesian optimisation. *arXiv preprint arXiv:1910.07779*, 2021.
- [55] Gonzalo Rios and Felipe Tobar. Compositionally-warped Gaussian processes. *Neural Networks*, 118:235–246, 2019.
- [56] Danilo Rezende and Shakir Mohamed. Variational inference with normalizing flows. In *Proceedings of the 32nd International Conference on Machine Learning*, volume 37, pages 1530–1538, 2015.
- [57] Juan Maronas, Oliver Hamelijnck, Jeremias Knoblauch, and Theodoros Damoulas. Transforming Gaussian processes with normalizing flows. *arXiv preprint arXiv:2011.01596*, 2020.
- [58] Vu Nguyen and Michael A Osborne. Knowing the what but not the where in Bayesian optimization. In *International Conference on Machine Learning*, pages 7317–7326, 2020.
- [59] Jasper Snoek, Kevin Swersky, Rich Zemel, and Ryan Adams. Input warping for Bayesian optimization of non-stationary functions. In *International Conference on Machine Learning*, pages 1674–1682, 2014.
- [60] Roberto Calandra, Jan Peters, Carl Edward Rasmussen, and Marc Peter Deisenroth. Manifold Gaussian processes for regression. In *2016 International Joint Conference on Neural Networks (IJCNN)*, pages 3338–3345. IEEE, 2016.
- [61] ChangYong Oh, Efstratios Gavves, and Max Welling. Bock: Bayesian optimization with cylindrical kernels. In *International Conference on Machine Learning*, pages 3868–3877, 2018.
- [62] Matthew Hoffman, Eric Brochu, and Nando de Freitas. Portfolio allocation for Bayesian optimization. In *Proceedings of the Twenty-Seventh Conference on Uncertainty in Artificial Intelligence*, pages 327–336, 2011.

- [63] Majid Abdolshah, Alistair Shilton, Santu Rana, Sunil Gupta, and Svetha Venkatesh. Multi-objective Bayesian optimisation with preferences over objectives. In *Advances in Neural Information Processing Systems*, volume 32, pages 12235–12245, 2019.
- [64] Chiwoo Park, David J Borth, Nicholas S Wilson, Chad N Hunter, and Fritz J Friedersdorf. Robust Gaussian process regression with a bias model. *arXiv preprint arXiv:2001.04639*, 2020.
- [65] Ilija Bogunovic, Jonathan Scarlett, Stefanie Jegelka, and Volkan Cevher. Adversarially robust optimization with Gaussian processes. In *Proceedings of the 32nd International Conference on Neural Information Processing Systems*, pages 5765–5775, 2018.
- [66] Dimitris Bertsimas, Omid Nohadani, and Kwong Meng Teo. Nonconvex robust optimization for problems with constraints. *INFORMS Journal on Computing*, 22(1):44–58, 2010.

## Checklist

1. For all authors...
  - (a) Do the main claims made in the abstract and introduction accurately reflect the paper’s contributions and scope? **[Yes]** Yes, we have studied common assumptions in BO, introduced a new algorithm that alleviates these issues and achieve SOTA across an extensive range of tasks.
  - (b) Did you describe the limitations of your work? **[Yes]** Yes, specifically in subsection 3.3 we emphasis these results are not indicative of the true multi-dimensional problem.
  - (c) Did you discuss any potential negative societal impacts of your work? **[Yes]** Yes, see Appendix A.
  - (d) Have you read the ethics review guidelines and ensured that your paper conforms to them? **[Yes]** I have read through and am certain we conform to all guidelines.
2. If you are including theoretical results...
  - (a) Did you state the full set of assumptions of all theoretical results? **[Yes]** See subsection B.3.
  - (b) Did you include complete proofs of all theoretical results? **[Yes]** See subsection B.3.
3. If you ran experiments...
  - (a) Did you include the code, data, and instructions needed to reproduce the main experimental results (either in the supplemental material or as a URL)? **[Yes]** We include the code in the supp material, and will upload it to GitHub once the review process is complete.
  - (b) Did you specify all the training details (e.g., data splits, hyperparameters, how they were chosen)? **[Yes]** Full experiment setup detailed in section 5. See Table 2 for search spaces for experiments.
  - (c) Did you report error bars (e.g., with respect to the random seed after running experiments multiple times)? **[Yes]** All experiments were conducted with 20 random seeds and error bars are shown in box-plots. See Figure 2, Figure 3, Figure 4 and Figure 5.
  - (d) Did you include the total amount of compute and the type of resources used (e.g., type of GPUs, internal cluster, or cloud provider)? **[No]** All experiments were conducted on a single multi-core machine. No GPU’s were required for these experiments hence we didn’t deem it relevant to describe computing power in the experiment section due to being able to run these experiments on a single laptop.
4. If you are using existing assets (e.g., code, data, models) or curating/releasing new assets...
  - (a) If your work uses existing assets, did you cite the creators? **[Yes]** See section 5 for full references to existing assets.
  - (b) Did you mention the license of the assets? **[No]** As all code used was open sourced.
  - (c) Did you include any new assets either in the supplemental material or as a URL? **[Yes]** Code included in the supplementary material.
  - (d) Did you discuss whether and how consent was obtained from people whose data you’re using/curating? **[No]** As not personal or private data was used, we only utilised UCI [17] open-sourced, readily accessible data.

- (e) Did you discuss whether the data you are using/curating contains personally identifiable information or offensive content? [No] No, as it does not contain any personally identifiable information or offensive content.
5. If you used crowdsourcing or conducted research with human subjects...
- (a) Did you include the full text of instructions given to participants and screenshots, if applicable? [No] As no research was conducted with human subjects.
  - (b) Did you describe any potential participant risks, with links to Institutional Review Board (IRB) approvals, if applicable? [No] As no research was conducted with human subjects.
  - (c) Did you include the estimated hourly wage paid to participants and the total amount spent on participant compensation? [No] As no research was conducted with human subjects.

## A Potential for Negative Societal Impact

With reference to the NeurIPS ethics guidelines our work is liable to have societal impact in deployed applications rather than as a standalone methodology. At its core, our contribution is to improve upon state-of-the-art performance in Bayesian optimisation for hyper-parameter tuning. Given that Bayesian optimisation is a general optimisation method it is possible that individuals may use the technique in ways that are damaging to society. This being said, it is highly unlikely that our research in itself will incite individuals to use Bayesian optimisation for these purposes.

## B Further Mathematical Details

### B.1 GP Posterior

Under a GP assumption with Gaussian-corrupted observations  $y_\ell = f(\mathbf{x}_\ell) + \epsilon_\ell$  where  $\epsilon_\ell \sim \mathcal{N}(0, \sigma^2)$ , and given a set  $\mathcal{D} = \{\mathbf{x}, \mathbf{y}\}$  of available data, the joint distribution of  $\mathcal{D}$  and an arbitrary set of input points  $\mathbf{x}_{1:q}$  is given by

$$\begin{bmatrix} \mathbf{y} \\ f(\mathbf{x}_{1:q}) \end{bmatrix} \middle| \boldsymbol{\theta} \sim \mathcal{N} \left( \begin{bmatrix} m(\mathbf{x}) \\ m(\mathbf{x}_{1:q}) \end{bmatrix}, \begin{bmatrix} \mathbf{K}_\theta + \sigma^2 \mathbf{I} & \mathbf{k}_\theta(\mathbf{x}_{1:q}) \\ \mathbf{k}_\theta^\top(\mathbf{x}_{1:q}) & \mathbf{k}_\theta(\mathbf{x}_{1:q}, \mathbf{x}_{1:q}) \end{bmatrix} \right),$$

where  $\mathbf{K}_\theta = \mathbf{K}_\theta(\mathbf{x}, \mathbf{x})$  and  $\mathbf{k}_\theta(\mathbf{x}_{1:q}) = \mathbf{k}_\theta(\mathbf{x}, \mathbf{x}_{1:q})$ . From this joint distribution one can derive through marginalisation [19] the predictive posterior  $p(f(\mathbf{x}_{1:q})|\mathcal{D}) = \mathcal{N}(\boldsymbol{\mu}_\theta(\mathbf{x}_{1:q}), \boldsymbol{\Sigma}_\theta(\mathbf{x}_{1:q}))$  with:

$$\begin{aligned} \boldsymbol{\mu}_\theta(\mathbf{x}_{1:q}) &= m(\mathbf{x}_{1:q}) + \mathbf{k}_\theta(\mathbf{x}_{1:q})^\top (\mathbf{K}_\theta + \sigma^2 \mathbf{I})^{-1} (\mathbf{y} - m(\mathbf{x})) \\ \boldsymbol{\Sigma}_\theta(\mathbf{x}_{1:q}) &= \mathbf{K}_\theta(\mathbf{x}_{1:q}, \mathbf{x}_{1:q}) - \mathbf{k}_\theta(\mathbf{x}_{1:q})^\top (\mathbf{K}_\theta + \sigma^2 \mathbf{I})^{-1} \mathbf{k}_\theta(\mathbf{x}_{1:q}) \end{aligned}$$

### B.2 Yeo-Johnson Transform

When labels take on arbitrary values, we use a Yeo-Johnson transform instead of Box-Cox. Such a transformation operates as follows:

$$\text{Y.J.}_\zeta(y_l) = \begin{cases} \frac{(y_l+1)^\zeta - 1}{\zeta}, & \text{if } \zeta \neq 0, y_l \geq 0 \\ \log(y_l + 1), & \text{if } \zeta = 0, y_l \geq 0 \\ \frac{(1-y_l)^{2-\zeta} - 1}{\zeta - 2}, & \text{if } \zeta \neq 2, y_l < 0 \\ -\log(1 - y_l), & \text{if } \zeta = 2, y_l < 0. \end{cases}$$

Analogous to the Box-Cox transform, the Yeo-Johnson's parameter is fit based on observed data solving the following 1-dimensional optimisation problem:

$$\max_{\zeta} -\frac{n}{2} \log \left[ \frac{\sum_{j=1}^n (\text{Y.J.}_\zeta(y_l) - \overline{\text{Y.J.}_\zeta(\mathbf{y})})^2}{n-1} \right] + (\zeta - 1) \sum_{i=1}^n [\text{sign}(y_l) \log(|y_l| + 1)],$$

with  $\overline{\text{Y.J.}_\zeta(\mathbf{y})}$  being the sample average computed after applying the Yeo-Johnson transformation.

### B.3 Robust Acquisition Objectives

Notice, the robust form of acquisition function given as  $\alpha_{\text{rob.}}(\mathbf{x}|\mathcal{D}) \equiv \mathbb{E}_{\epsilon \sim \mathcal{N}(\mathbf{0}, \sigma^2 \mathbf{I})} [\alpha^{\theta+\epsilon}(\mathbf{x}|\mathcal{D})]$  constitutes an intractable integral. Therefore, in order to be maximised during BO execution, it should be replaced with accurate approximation. Our next result establishes such arbitrary accurate approximation with high probability.

**Lemma:** Let  $\delta \in (0, 1)$  be a desirable probability threshold, and  $\rho \in (0, 1)$  be a desirable accuracy parameter. Consider the GP process with mean function  $m(\mathbf{x})$  and covariance function  $k_\theta(\mathbf{x}, \mathbf{x}')$  such that  $\forall \mathbf{x}, \mathbf{x}' \in \mathcal{X}, \boldsymbol{\theta} \in \mathbb{R}^P$ :

$$\begin{aligned} |k_\theta(\mathbf{x}, \mathbf{x})| &\geq M_0, \quad |k_\theta(\mathbf{x}, \mathbf{x}')| \leq M_1, \\ \|\nabla_{\boldsymbol{\theta}} k_\theta(\mathbf{x}, \mathbf{x}')\|_2 &\leq M_2, \quad |m(\mathbf{x})| \leq M_4. \end{aligned} \tag{3}$$



Moreover, assume that observations  $y \in \mathcal{D}$  are bounded, i.e.  $|y| \leq C$  and let  $\bar{\alpha}^\theta(\mathbf{x}|\mathcal{D}) = \alpha^\theta(\mathbf{x}|\mathcal{D}) + \eta\sigma_n$  with  $\eta$  being standard normal random variable. Then, there are constants  $c_1$  and  $c_2$ , such that choosing  $\sigma_n \leq c_1$  and  $\sigma_\epsilon \leq c_2$ :

$$|\bar{\alpha}^\theta(\mathbf{x}|\mathcal{D}) - \mathbb{E}_{\epsilon \sim \mathcal{N}(\mathbf{0}, \sigma_\epsilon^2 \mathbf{I})} [\alpha^{\theta+\epsilon}(\mathbf{x}|\mathcal{D})]| \leq \rho.$$

with probability at least  $1 - \delta$ .

*Proof.* Without loss of generality we chose UCB acquisition function  $\alpha(\mathbf{x})^\theta(\mathbf{x}|\mathcal{D}) = \alpha_{\text{UCB}}(\mathbf{x})^\theta(\mathbf{x}|\mathcal{D})$  and to avoid technical complications related to multivariate calculus we consider batch size  $q = 1$ . In this case, UCB acquisition function can be written as  $\alpha_{\text{UCB}}(\mathbf{x})^\theta(\mathbf{x}|\mathcal{D}) = \mu_\theta(\mathbf{x}|\mathcal{D}) + \sqrt{\frac{\beta\pi}{2}}\sigma_\theta(\mathbf{x}|\mathcal{D})$ , where  $\mu_\theta(\mathbf{x}|\mathcal{D})$  and  $\sigma_\theta(\mathbf{x}|\mathcal{D})$  are posterior mean and posterior deviation respectively. Consider a Monte-Carlo estimation of  $\alpha_{\text{rob.}}(\mathbf{x}|\mathcal{D}) \equiv \mathbb{E}_{\epsilon \sim \mathcal{N}(\mathbf{0}, \sigma_\epsilon^2 \mathbf{I})} [\alpha^{\theta+\epsilon}(\mathbf{x}|\mathcal{D})]$ :

$$\hat{\alpha}^\theta(\mathbf{x}|\mathcal{D}) = \frac{1}{N_\epsilon} \sum_{j=1}^{N_\epsilon} \alpha^{\theta+\epsilon_j}(\mathbf{x}|\mathcal{D})$$

where  $\epsilon_j$  are i.i.d. samples drawn from  $\mathcal{N}(\mathbf{0}, \sigma_\epsilon^2 \mathbf{I})$ . Then, adding and subtracting  $\hat{\alpha}^\theta(\mathbf{x}|\mathcal{D})$  gives:

$$\begin{aligned} & |\bar{\alpha}^\theta(\mathbf{x}|\mathcal{D}) - \mathbb{E}_{\epsilon \sim \mathcal{N}(\mathbf{0}, \sigma_\epsilon^2 \mathbf{I})} [\alpha^{\theta+\epsilon}(\mathbf{x}|\mathcal{D})]| \leq \\ & |\bar{\alpha}^\theta(\mathbf{x}|\mathcal{D}) - \hat{\alpha}^\theta(\mathbf{x}|\mathcal{D})| + |\hat{\alpha}^\theta(\mathbf{x}|\mathcal{D}) - \mathbb{E}_{\epsilon \sim \mathcal{N}(\mathbf{0}, \sigma_\epsilon^2 \mathbf{I})} [\alpha^{\theta+\epsilon}(\mathbf{x}|\mathcal{D})]|. \end{aligned}$$

Using definition of  $\hat{\alpha}^\theta(\mathbf{x}|\mathcal{D})$  in the above result gives:

$$\begin{aligned} & |\bar{\alpha}^\theta(\mathbf{x}|\mathcal{D}) - \mathbb{E}_{\epsilon \sim \mathcal{N}(\mathbf{0}, \sigma_\epsilon^2 \mathbf{I})} [\alpha^{\theta+\epsilon}(\mathbf{x}|\mathcal{D})]| \leq \\ & \frac{1}{N_\epsilon} \sum_{j=1}^{N_\epsilon} |\bar{\alpha}^\theta(\mathbf{x}|\mathcal{D}) - \alpha^{\theta+\epsilon_j}(\mathbf{x}|\mathcal{D})| + \left| \frac{1}{N_\epsilon} \sum_{j=1}^{N_\epsilon} \alpha^{\theta+\epsilon_j}(\mathbf{x}|\mathcal{D}) - \mathbb{E}_{\epsilon \sim \mathcal{N}(\mathbf{0}, \sigma_\epsilon^2 \mathbf{I})} [\alpha^{\theta+\epsilon}(\mathbf{x}|\mathcal{D})] \right| \end{aligned} \quad (4)$$

Let us study separately each term in the above result. Applying the Chebyshev inequality for the second term in the above expression, we have that with probability at least  $p_1 = 1 - \frac{8[\mathbb{E}_\epsilon [\mu_{\theta+\epsilon}^2(\mathbf{x}|\mathcal{D})] + \frac{\beta\pi}{2}\mathbb{E}_\epsilon [\sigma_{\theta+\epsilon}^2(\mathbf{x}|\mathcal{D})]]}{N_\epsilon \rho^2}$ :

$$\left| \frac{1}{N_\epsilon} \sum_{j=1}^{N_\epsilon} \alpha^{\theta+\epsilon_j}(\mathbf{x}|\mathcal{D}) - \mathbb{E}_{\epsilon \sim \mathcal{N}(\mathbf{0}, \sigma_\epsilon^2 \mathbf{I})} [\alpha^{\theta+\epsilon}(\mathbf{x}|\mathcal{D})] \right| \leq \frac{\rho}{2}. \quad (5)$$

In order to ensure that  $p_1 = 1 - \frac{\delta}{2}$  the number of samples  $\epsilon_j$  should be taken:

$$N_\epsilon = \left\lceil \frac{16 \left[ \mathbb{E}_\epsilon [\mu_{\theta+\epsilon}^2(\mathbf{x}|\mathcal{D})] + \frac{\beta\pi}{2} \mathbb{E}_\epsilon [\sigma_{\theta+\epsilon}^2(\mathbf{x}|\mathcal{D})] \right]}{\delta \rho^2} \right\rceil.$$

We will simplify this expression using bounds in (3) later. Now, let us focus on the second term in (4). To bound it, we are going to establish a bound on  $|\bar{\alpha}^\theta(\mathbf{x}|\mathcal{D}) - \alpha^{\theta+\epsilon_j}(\mathbf{x}|\mathcal{D})|$ . For small random perturbation  $\epsilon_j$  we have (with probability 1):

$$\begin{aligned} \alpha^{\theta+\epsilon_j}(\mathbf{x}|\mathcal{D}) &= \alpha^\theta(\mathbf{x}|\mathcal{D}) + \epsilon_j^\top \nabla_\theta \alpha^\theta(\mathbf{x}|\mathcal{D}) + o(\|\epsilon_j\|) = \\ &= \alpha^\theta(\mathbf{x}|\mathcal{D}) + \epsilon_j^\top \nabla_\theta \left[ \mu_\theta(\mathbf{x}|\mathcal{D}) + \sqrt{\frac{\beta\pi}{2}} \sigma_\theta(\mathbf{x}|\mathcal{D}) \right] + o(\|\epsilon_j\|_2). \end{aligned}$$

Let us denote

$$\mathbf{h}_\theta(\mathbf{x}|\mathcal{D}) = \nabla_\theta \left[ \mu_\theta(\mathbf{x}|\mathcal{D}) + \sqrt{\frac{\beta\pi}{2}} \sigma_\theta(\mathbf{x}|\mathcal{D}) \right]$$

then, using the Cauchy–Schwarz inequality we have:

$$|\alpha^{\theta+\epsilon_j}(\mathbf{x}|\mathcal{D}) - \alpha^\theta(\mathbf{x}|\mathcal{D})| \leq \|\epsilon_j\|_2 \|\mathbf{h}_\theta(\mathbf{x}|\mathcal{D})\|_2 + o(1)$$

Since  $\epsilon_j \sim \mathcal{N}(0, 1)$ , then with probability at least  $1 - \frac{\delta}{4N_\epsilon}$ :

$$\|\epsilon_j\|_2 \leq 4\sigma_\epsilon\sqrt{p} + 2\sigma_\epsilon\sqrt{\log \frac{4N_\epsilon}{\delta}}$$

Let us assume (and later we will prove the existence of such bound) that  $\|\mathbf{h}_\theta(\mathbf{x}|\mathcal{D})\|_2 \leq A_1$ . Then, with probability at least  $1 - \frac{\delta}{4N_\epsilon}$ :

$$|\alpha^{\theta+\epsilon_j}(\mathbf{x}|\mathcal{D}) - \alpha^\theta(\mathbf{x}|\mathcal{D})| \leq \left[ 4\sigma_\epsilon\sqrt{p} + 2\sigma_\epsilon\sqrt{\log \frac{4N_\epsilon}{\delta}} \right] [A_1 + o(1)]$$

On the other hand, for  $\bar{\alpha}^\theta(\mathbf{x}|\mathcal{D}) = \alpha^\theta(\mathbf{x}|\mathcal{D}) + \eta\sigma_\eta$  with probability at least  $1 - \frac{\delta}{4N_\epsilon}$  we have:

$$|\bar{\alpha}^\theta(\mathbf{x}|\mathcal{D}) - \alpha^\theta(\mathbf{x}|\mathcal{D})| \leq \Phi^{-1} \left( 1 - \frac{\delta}{8N_\epsilon} \right) \sigma_n.$$

where  $\Phi(\cdot)$  is cumulative distribution function for standard Gaussian variable. Hence, by choosing  $\sigma_\epsilon = \min \left\{ 1, \frac{\Phi^{-1} \left( 1 - \frac{\delta}{8N_\epsilon} \right) \sigma_n}{\left[ 4\sqrt{p} + 2\sqrt{\log \frac{4N_\epsilon}{\delta}} \right] [A_1 + o(1)]} \right\}$  with probability at least  $1 - \frac{\delta}{2N_\epsilon}$  we have that both  $\bar{\alpha}^\theta(\mathbf{x}|\mathcal{D})$  and  $\alpha^{\theta+\epsilon_j}(\mathbf{x}|\mathcal{D})$  belong to the interval centred at  $\alpha^\theta(\mathbf{x}|\mathcal{D})$  of size  $\Phi^{-1} \left( 1 - \frac{\delta}{8N_\epsilon} \right) \sigma_n$ . Therefore, with probability at least  $1 - \frac{\delta}{2N_\epsilon}$ :

$$|\bar{\alpha}^\theta(\mathbf{x}|\mathcal{D}) - \alpha^{\theta+\epsilon_j}(\mathbf{x}|\mathcal{D})| \leq 2\Phi^{-1} \left( 1 - \frac{\delta}{8N_\epsilon} \right) \sigma_n$$

Hence, by choosing  $\sigma_n = \frac{\rho}{4\Phi^{-1} \left( 1 - \frac{\delta}{8N_\epsilon} \right)}$  we arrive:

$$|\bar{\alpha}^\theta(\mathbf{x}|\mathcal{D}) - \alpha^{\theta+\epsilon_j}(\mathbf{x}|\mathcal{D})| \leq \frac{\rho}{2}$$

and, therefore, for the first term in (4) with probability at least  $1 - \frac{\delta}{2}$  we have:

$$\frac{1}{N_\epsilon} \sum_{j=1}^{N_\epsilon} |\bar{\alpha}^\theta(\mathbf{x}|\mathcal{D}) - \alpha^{\theta+\epsilon_j}(\mathbf{x}|\mathcal{D})| \leq \frac{\rho}{2}$$

Combining this result with (5) gives, that with probability at least  $1 - \delta$  we have:

$$|\bar{\alpha}^\theta(\mathbf{x}|\mathcal{D}) - \mathbb{E}_{\epsilon \sim \mathcal{N}(\mathbf{0}, \sigma_\epsilon^2 \mathbf{I})} [\alpha^{\theta+\epsilon}(\mathbf{x}|\mathcal{D})]| \leq \rho$$

upon the following setup:

$$\sigma_n = \frac{\rho}{4\Phi^{-1} \left( 1 - \frac{\delta}{8N_\epsilon} \right)}, \quad \sigma_\epsilon = \min \left\{ 1, \frac{\rho}{8 \left[ 2\sqrt{p} + \sqrt{\log \frac{4N_\epsilon}{\delta}} \right] [A_1 + o(1)]} \right\}, \quad (6)$$

with

$$N_\epsilon = \left\lceil \frac{16 \left[ \mathbb{E}_\epsilon [\mu_{\theta+\epsilon}^2(\mathbf{x}|\mathcal{D})] + \frac{\beta\pi}{2} \mathbb{E}_\epsilon [\sigma_{\theta+\epsilon}^2(\mathbf{x}|\mathcal{D})] \right]}{\delta\rho^2} \right\rceil.$$

Our last step is to prove the existence of constant  $A_1$  such that  $\|\mathbf{h}_\theta(\mathbf{x})\|_2 \leq A_1$  and also to simplify these expressions by deriving bounds on  $\mathbb{E}_\epsilon [\mu_{\theta+\epsilon}(\mathbf{x}|\mathcal{D})]$  and  $\mathbb{E}_\epsilon [\sigma_{\theta+\epsilon}^2(\mathbf{x}|\mathcal{D})]$ . This will be provided as a separate Claim:

Claim: Let bounds in (3) hold, then there are positive constants  $A_1, A_2$  and  $A_3$ , such that:

$$\|\mathbf{h}_\theta(\mathbf{x})\|_2 \leq A_1, \quad \mathbb{E}_\epsilon [\mu_{\theta+\epsilon}(\mathbf{x}|\mathcal{D})] \leq A_2, \quad \mathbb{E}_\epsilon [\sigma_{\theta+\epsilon}^2(\mathbf{x}|\mathcal{D})] \leq A_3. \quad (7)$$

*Proof.* We start with bound on  $\|\mathbf{h}_\theta(\mathbf{x})\|_2$ . Let us denote for simplicity  $\mathbf{a}_\theta = [k_\theta(\mathbf{x}, \mathbf{x}_i)]_{\mathbf{x}_i \in \mathcal{D}}$ ,  $\mathbf{B}_\theta = \left[ [k_\theta(\mathbf{x}, \mathbf{x}')]_{\mathbf{x} \in \mathcal{D}, \mathbf{x}' \in \mathcal{D}} + \mathbf{I} \right]^{-1}$ ,  $\mathbf{y} = [y(\mathbf{x})]_{\mathbf{x} \in \mathcal{D}}$ ,  $\mathbf{m}_\mathcal{D} = [m(\mathbf{x})]_{\mathbf{x} \in \mathcal{D}}$ ,  $m = m(\mathbf{x})$ , and  $k_\theta = k_\theta(\mathbf{x}, \mathbf{x})$ , then

$$\mu_\theta(\mathbf{x}|\mathcal{D}) = \mathbf{a}_\theta^\top \mathbf{B}_\theta [\mathbf{y} - \mathbf{m}_\mathcal{D}] + m, \quad \sigma_\theta^2(\mathbf{x}|\mathcal{D}) = \mathbf{a}_\theta^\top \mathbf{B}_\theta \mathbf{a}_\theta + k_\theta$$

Let us also denote the size of  $\mathcal{D}$  as  $N$ , then: have:

$$\begin{aligned} \nabla_\theta \mu_\theta(\mathbf{x}|\mathcal{D}) &= \sum_{i=1}^N \sum_{j=1}^N \nabla_\theta [[y_j - m_j][\mathbf{a}_\theta]_i [\mathbf{B}_\theta]_{ij}] = \\ &= \sum_{i=1}^N \sum_{j=1}^N [[y_j - m_j][\mathbf{B}_\theta]_{ij} \nabla_\theta [\mathbf{a}_\theta]_i] + \sum_{i=1}^N \sum_{j=1}^N [[y_j - m_j][\mathbf{a}_\theta]_i \nabla_\theta [[\mathbf{B}_\theta]_{ij}]] \end{aligned}$$

Consider each term in this expression separately:

$$\begin{aligned} \left\| \sum_{i=1}^N \sum_{j=1}^N [y_j - m_j][\mathbf{B}_\theta]_{ij} \nabla_\theta [\mathbf{a}_\theta]_i \right\|_2 &= \left\| \sum_{i=1}^N [\mathbf{B}_\theta [\mathbf{y} - \mathbf{m}_\mathcal{D}]]_i \nabla_\theta [\mathbf{a}_\theta]_i \right\|_2 \leq \\ &= \sum_{i=1}^N \|\mathbf{B}_\theta(i, :)\|_2 \|\mathbf{y} - \mathbf{m}_\mathcal{D}\|_2 \|\nabla_\theta [\mathbf{a}_\theta]_i\|_2 \end{aligned}$$

Using  $|y| \leq C$  and  $|m(\mathbf{x})| \leq M_4$  we have  $\|\mathbf{y} - \mathbf{m}_\mathcal{D}\|_2 \leq (C + M_4)\sqrt{N}$  and  $\|\nabla_\theta [\mathbf{a}_\theta]_i\|_2 \leq M_2$  we have:

$$\begin{aligned} \left\| \sum_{i=1}^N \sum_{j=1}^N [y_j - m_j][\mathbf{B}_\theta]_{ij} \nabla_\theta [\mathbf{a}_\theta]_i \right\|_2 &\leq (C + M_4)\sqrt{N} \sum_{i=1}^N \|\mathbf{B}_\theta(i, :)\|_2 \|\nabla_\theta [\mathbf{a}_\theta]_i\|_2 \leq \quad (8) \\ (C + M_4)\sqrt{N} \|\mathbf{B}_\theta\|_F \sum_{i=1}^N \|\nabla_\theta [\mathbf{a}_\theta]_i\|_2 &\leq (C + M_4)\sqrt{N} \sqrt{\text{rank}(\mathbf{B}_\theta) \|\mathbf{B}_\theta\|_2} \sum_{i=1}^N \|\nabla_\theta [\mathbf{a}_\theta]_i\|_2 \leq \\ \frac{(C + M_4)N}{\sigma_n^2} \sum_{i=1}^N \|\nabla_\theta [\mathbf{a}_\theta]_i\|_2 &= \frac{(C + M_4)N^2 M_2}{\sigma_n^2} \end{aligned}$$

Now, let us consider the second term in the expression for the posterior mean:

$$\sum_{i=1}^N \sum_{j=1}^N [y_j - m_j][\mathbf{a}_\theta]_i \nabla_\theta [[\mathbf{B}_\theta]_{ij}] = \sum_{i=1}^N [\mathbf{a}_\theta]_i \left[ \sum_{j=1}^N [y_j - m_j] \nabla_\theta [[\mathbf{B}_\theta]_{ij}] \right]$$

Notice, that the gradient expression above is presented in a form of a vector:

$$\nabla_\theta [[\mathbf{B}_\theta]_{ij}] = \begin{bmatrix} \frac{\partial}{\partial \theta_1} [\mathbf{K}_\theta + \sigma_n \mathbf{I}]_{ij}^{-1}, \\ \vdots \\ \frac{\partial}{\partial \theta_p} [\mathbf{K}_\theta + \sigma_n \mathbf{I}]_{ij}^{-1} \end{bmatrix}$$

where we use notation  $\mathbf{K}_\theta = [k_\theta(\mathbf{x}_i, \mathbf{x}_j)]_{i=1, j=1}^{N, N}$ . For the  $r^{th}$  component we have:

$$\frac{\partial}{\partial \theta_r} [\mathbf{K}_\theta + \sigma_n \mathbf{I}]_{ij}^{-1} = \left[ -[\mathbf{K}_\theta + \sigma_n \mathbf{I}]^{-1} \frac{\partial}{\partial \theta_r} [\mathbf{K}_\theta + \sigma_n \mathbf{I}] [\mathbf{K}_\theta + \sigma_n \mathbf{I}]^{-1} \right]_{ij} \quad (9)$$

Now we can study the gradient of the second term in the posterior mean expression:

$$\begin{aligned} \left\| \sum_{i=1}^N [\mathbf{a}_\theta]_i \left[ \sum_{j=1}^N [y_j - m_j] \nabla_\theta [[\mathbf{B}_\theta]_{ij}] \right] \right\|_2 &\leq \sum_{i=1}^N |[\mathbf{a}_\theta]_i| \left[ \sum_{j=1}^N \|\mathbf{y} - \mathbf{m}_\mathcal{D}\|_2 \|\nabla_\theta [[\mathbf{B}_\theta]_{ij}]\|_2 \right] \leq \\ (C + M_4)\sqrt{N} M_1 \sum_{i=1}^N \sum_{j=1}^N \sum_{r=1}^p \left| \frac{\partial}{\partial \theta_r} [\mathbf{K}_\theta + \sigma_n \mathbf{I}]_{ij}^{-1} \right| & \end{aligned}$$

Using result (9) in the above expression we have:

$$\begin{aligned}
& \left\| \sum_{i=1}^N [\mathbf{a}_\theta]_i \left[ \sum_{j=1}^N [y_j - m_j] \nabla_{\boldsymbol{\theta}} [[\mathbf{B}_\theta]_{ij}] \right] \right\|_2 \leq \\
& (C + M_4) \sqrt{N} M_1 \sum_{i=1}^N \sum_{j=1}^N \sum_{r=1}^p \left| \frac{\partial}{\partial \theta_r} [\mathbf{K}_\theta + \sigma_n \mathbf{I}]_{ij}^{-1} \right| \leq \\
& (C + M_4) \sqrt{N} M_1 \sum_{r=1}^p \sum_{i=1}^N \sum_{j=1}^N \left| \frac{\partial}{\partial \theta_r} [\mathbf{K}_\theta + \sigma_n \mathbf{I}]_{ij}^{-1} \right| \leq \\
& (C + M_4) N \sqrt{N} M_1 \times \sum_{r=1}^p \left\| [\mathbf{K}_\theta + \sigma_n \mathbf{I}]^{-1} \frac{\partial}{\partial \theta_r} [\mathbf{K}_\theta + \sigma_n \mathbf{I}] [\mathbf{K}_\theta + \sigma_n \mathbf{I}]^{-1} \right\|_F
\end{aligned}$$

where we used that  $\sum_{i=1}^N \sum_{j=1}^N |C_{ij}| \leq N \|C\|_F$  for any arbitrary matrix  $C \in \mathbb{R}^{N \times N}$ . Because  $\frac{\partial}{\partial \theta_r} [\mathbf{K}_\theta + \sigma_n \mathbf{I}] = \frac{\partial}{\partial \theta_r} \mathbf{K}_\theta$ . Therefore:

$$\begin{aligned}
& \frac{\left\| \sum_{i=1}^N [\mathbf{a}_\theta]_i \left[ \sum_{j=1}^N [y_j - m_j] \nabla_{\boldsymbol{\theta}} [[\mathbf{B}_\theta]_{ij}] \right] \right\|_2}{(C + M_4) N \sqrt{N} M_1} \leq \\
& \sum_{r=1}^p \left\| [\mathbf{K}_\theta + \sigma_n \mathbf{I}]^{-1} \frac{\partial}{\partial \theta_r} \mathbf{K}_\theta [\mathbf{K}_\theta + \sigma_n \mathbf{I}]^{-1} \right\|_F \leq \\
& \sqrt{N} \sum_{r=1}^p \left\| [\mathbf{K}_\theta + \sigma_n \mathbf{I}]^{-1} \frac{\partial}{\partial \theta_r} \mathbf{K}_\theta [\mathbf{K}_\theta + \sigma_n \mathbf{I}]^{-1} \right\|_2
\end{aligned}$$

Using properties of matrix 2-norm  $\|\cdot\|_2$ :

$$\left\| [\mathbf{K}_\theta + \sigma_n \mathbf{I}]^{-1} \right\|_2 \leq \frac{1}{\sigma_n^2}$$

Hence,

$$\begin{aligned}
& \frac{\left\| \sum_{i=1}^N [\mathbf{a}_\theta]_i \left[ \sum_{j=1}^N [y_j - m_j] \nabla_{\boldsymbol{\theta}} [[\mathbf{B}_\theta]_{ij}] \right] \right\|_2}{(C + M_4) N^2 M_1} \leq \\
& \sum_{r=1}^p \left\| [\mathbf{K}_\theta + \sigma_n \mathbf{I}]^{-1} \right\|_2 \left\| \frac{\partial}{\partial \theta_r} \mathbf{K}_\theta \right\|_2 \left\| [\mathbf{K}_\theta + \sigma_n \mathbf{I}]^{-1} \right\|_2 \leq \frac{1}{\sigma_n^4} \sum_{r=1}^p \left\| \frac{\partial}{\partial \theta_r} \mathbf{K}_\theta \right\|_2.
\end{aligned} \tag{10}$$

Let us study the last term in the above expression. Using  $\sqrt{c_1^2 + \dots + c_R^2} \leq |c_1| + \dots + |c_R|$  for any set of real numbers  $c_1, \dots, c_R \in \mathbb{R}$  we have:

$$\begin{aligned}
& \left\| \frac{\partial}{\partial \theta_r} \mathbf{K}_\theta \right\|_2 = \left\| \begin{bmatrix} \frac{\partial}{\partial \theta_r} k_\theta(\mathbf{x}_1, \mathbf{x}_1), & \dots & \frac{\partial}{\partial \theta_r} k_\theta(\mathbf{x}_1, \mathbf{x}_N) \\ \vdots & \ddots & \vdots \\ \frac{\partial}{\partial \theta_r} k_\theta(\mathbf{x}_N, \mathbf{x}_1), & \dots & \frac{\partial}{\partial \theta_r} k_\theta(\mathbf{x}_N, \mathbf{x}_N) \end{bmatrix} \right\|_2 \leq \\
& \left\| \begin{bmatrix} \frac{\partial}{\partial \theta_r} k_\theta(\mathbf{x}_1, \mathbf{x}_1), & \dots & \frac{\partial}{\partial \theta_r} k_\theta(\mathbf{x}_1, \mathbf{x}_N) \\ \vdots & \ddots & \vdots \\ \frac{\partial}{\partial \theta_r} k_\theta(\mathbf{x}_N, \mathbf{x}_1), & \dots & \frac{\partial}{\partial \theta_r} k_\theta(\mathbf{x}_N, \mathbf{x}_N) \end{bmatrix} \right\|_F = \\
& \sqrt{\sum_{i=1}^N \sum_{j=1}^N \left[ \frac{\partial}{\partial \theta_r} k_\theta(\mathbf{x}_i, \mathbf{x}_j) \right]^2} \leq \sum_{i=1}^N \sum_{j=1}^N \left| \frac{\partial}{\partial \theta_r} k_\theta(\mathbf{x}_i, \mathbf{x}_j) \right|
\end{aligned}$$

Substituting this expression in (10) gives us:

$$\begin{aligned} \left\| \frac{\sum_{i=1}^N [\mathbf{a}_\theta]_i \left[ \sum_{j=1}^N [y_j - m_j] \nabla_\theta [\mathbf{B}_\theta]_{ij} \right]}{(C + M_4) N^2 M_1} \right\|_2 &\leq \frac{1}{\sigma_n^4} \sum_{r=1}^d \sum_{i=1}^N \sum_{j=1}^N \left| \frac{\partial}{\partial \theta_r} k_\theta(\mathbf{x}_i, \mathbf{x}_j) \right| \leq \\ \frac{\sqrt{p}}{\sigma_n^4} \sum_{i=1}^N \sum_{j=1}^N \|\nabla_\theta k_\theta(\mathbf{x}_i, \mathbf{x}_j)\|_2 &\leq \frac{N^2 \sqrt{p} M_2}{\sigma_n^4}. \end{aligned} \quad (11)$$

Hence, combining results (8) and (11) we have:

$$\|\nabla_\theta \mu_\theta(\mathbf{x}|\mathcal{D})\|_2 \leq \frac{(C + M_4) N^2 M_2}{\sigma_n^2} \left[ 1 + \frac{N^2 M_1 \sqrt{p}}{\sigma_n^2} \right] \quad (12)$$

Now, let us focus on the gradient of the posterior deviation:

$$\begin{aligned} \nabla_\theta \sigma_\theta(\mathbf{x}|\mathcal{D}) &= \nabla_\theta \left[ \sqrt{k_\theta(\mathbf{x}, \mathbf{x}) - \mathbf{a}_\theta^\top [\mathbf{K}_\theta + \sigma_n^2 \mathbf{I}]^{-1} \mathbf{a}_\theta} \right] = \\ \frac{1}{2\sigma_\theta(\mathbf{x}|\mathcal{D})} \nabla_\theta [k_\theta(\mathbf{x}, \mathbf{x}) - \mathbf{a}_\theta^\top [\mathbf{K}_\theta + \sigma_n^2 \mathbf{I}]^{-1} \mathbf{a}_\theta] &= \frac{1}{2\sigma_\theta(\mathbf{x})} [\nabla_\theta k_\theta(\mathbf{x}, \mathbf{x}) - \nabla_\theta [\mathbf{a}_\theta^\top [\mathbf{K}_\theta + \sigma_n^2 \mathbf{I}]^{-1} \mathbf{a}_\theta]] \end{aligned}$$

Let us study the second gradient expression. Using our notation we have:

$$\mathbf{a}_\theta^\top [\mathbf{K}_\theta + \sigma_n^2 \mathbf{I}]^{-1} \mathbf{a}_\theta = \mathbf{a}_\theta^\top \mathbf{B}_\theta \mathbf{a}_\theta = \sum_{i=1}^N \sum_{j=1}^N [\mathbf{a}_\theta]_i [\mathbf{a}_\theta]_j [\mathbf{B}_\theta]_{ij}$$

Hence, for the gradient we have:

$$\begin{aligned} \nabla_\theta [\mathbf{a}_\theta^\top \mathbf{B}_\theta \mathbf{a}_\theta] &= \sum_{i=1}^N \sum_{j=1}^N \nabla_\theta [[\mathbf{a}_\theta]_i [\mathbf{a}_\theta]_j [\mathbf{B}_\theta]_{ij}] = \\ \sum_{i=1}^N \sum_{j=1}^N \nabla_\theta [[\mathbf{a}_\theta]_i] [\mathbf{a}_\theta]_j [\mathbf{B}_\theta]_{ij} &+ \sum_{i=1}^N \sum_{j=1}^N \nabla_\theta [[\mathbf{a}_\theta]_j] [\mathbf{a}_\theta]_i [\mathbf{B}_\theta]_{ij} + \\ \sum_{i=1}^N \sum_{j=1}^N \nabla_\theta [[\mathbf{B}_\theta]_{ij}] [\mathbf{a}_\theta]_i [\mathbf{a}_\theta]_j. \end{aligned}$$

Hence, for the norm of the above expression we have:

$$\begin{aligned} \|\nabla_\theta [\mathbf{a}_\theta^\top \mathbf{B}_\theta \mathbf{a}_\theta]\|_2 &= \sum_{i=1}^N \sum_{j=1}^N \nabla_\theta [[\mathbf{a}_\theta]_i [\mathbf{a}_\theta]_j [\mathbf{B}_\theta]_{ij}] = \\ \sum_{i=1}^N \sum_{j=1}^N \left\| \nabla_\theta [[\mathbf{B}_\theta]_{ij}] \right\|_2 &|[\mathbf{a}_\theta]_i [\mathbf{a}_\theta]_j| + \sum_{i=1}^N \sum_{j=1}^N \|\nabla_\theta\|_2 \left| [[\mathbf{a}_\theta]_i] [\mathbf{a}_\theta]_j [\mathbf{B}_\theta]_{ij} \right| + \\ \sum_{i=1}^N \sum_{j=1}^N \|\nabla_\theta [[\mathbf{a}_\theta]_j]\|_2 &\left| [\mathbf{a}_\theta]_i [\mathbf{B}_\theta]_{ij} \right|. \end{aligned}$$

Let us bound each term in this expression:

1. The first term:

$$\begin{aligned} \sum_{i=1}^N \sum_{j=1}^N \left\| \nabla_\theta [[\mathbf{B}_\theta]_{ij}] \right\|_2 &|[\mathbf{a}_\theta]_i [\mathbf{a}_\theta]_j| \leq \\ \sum_{i=1}^N \sum_{j=1}^N \left\| \nabla_\theta [[\mathbf{B}_\theta]_{ij}] \right\|_2 &\|\mathbf{a}_\theta\|_2 \|\mathbf{a}_\theta\|_2 \leq M_1^2 \sum_{i=1}^N \sum_{j=1}^N \left\| \nabla_\theta [[\mathbf{B}_\theta]_{ij}] \right\|_2 \end{aligned}$$

Using previous bound for  $\left\| \nabla_{\boldsymbol{\theta}} [\mathbf{B}_{\boldsymbol{\theta}}]_{ij} \right\|_2$  we have:

$$\begin{aligned} \sum_{i=1}^N \sum_{j=1}^N \left\| \nabla_{\boldsymbol{\theta}} [\mathbf{B}_{\boldsymbol{\theta}}]_{ij} \right\|_2 |[\mathbf{a}_{\boldsymbol{\theta}}]_i [\mathbf{a}_{\boldsymbol{\theta}}]_j| &\leq M_1^2 \sum_{i=1}^N \sum_{j=1}^N \sum_{r=1}^p \left| \frac{\partial}{\partial \theta_r} [\mathbf{K}_{\boldsymbol{\theta}} + \sigma_n^2 \mathbf{I}]_{ij}^{-1} \right| = \\ &NM_1^2 \sum_{r=1}^p \left\| [\mathbf{K}_{\boldsymbol{\theta}} + \sigma_n \mathbf{I}]^{-1} \frac{\partial}{\partial \theta_r} \mathbf{K}_{\boldsymbol{\theta}} [\mathbf{K}_{\boldsymbol{\theta}} + \sigma_n \mathbf{I}]^{-1} \right\|_F \leq \\ &N^{\frac{3}{2}} M_1^2 \sum_{r=1}^p \left\| [\mathbf{K}_{\boldsymbol{\theta}} + \sigma_n \mathbf{I}]^{-1} \frac{\partial}{\partial \theta_r} \mathbf{K}_{\boldsymbol{\theta}} [\mathbf{K}_{\boldsymbol{\theta}} + \sigma_n \mathbf{I}]^{-1} \right\|_2 \end{aligned}$$

Since  $\left\| [\mathbf{K}_{\boldsymbol{\theta}} + \sigma_n \mathbf{I}]^{-1} \right\|_2 \leq \frac{1}{\sigma_n^2}$  we have:

$$\sum_{i=1}^N \sum_{j=1}^N \left\| \nabla_{\boldsymbol{\theta}} [\mathbf{B}_{\boldsymbol{\theta}}]_{ij} \right\|_2 |[\mathbf{a}_{\boldsymbol{\theta}}]_i [\mathbf{a}_{\boldsymbol{\theta}}]_j| \leq \frac{N\sqrt{N}M_1^2}{\sigma_n^4} \sum_{r=1}^p \sum_{i=1}^N \sum_{j=1}^N \left| \frac{\partial}{\partial \theta_r} k_{\boldsymbol{\theta}}(\mathbf{x}_i, \mathbf{x}_j) \right|.$$

Using  $\sum_{r=1}^p \sum_{i=1}^N \sum_{j=1}^N \left| \frac{\partial}{\partial \theta_r} k_{\boldsymbol{\theta}}(\mathbf{x}_i, \mathbf{x}_j) \right| = \sqrt{p} \sum_{i=1}^N \sum_{j=1}^N \|\nabla_{\boldsymbol{\theta}} k_{\boldsymbol{\theta}}(\mathbf{x}_i, \mathbf{x}_j)\|_2 \leq N^2 \sqrt{p} M_2$ , we have:

$$\sum_{i=1}^N \sum_{j=1}^N \left\| \nabla_{\boldsymbol{\theta}} [\mathbf{B}_{\boldsymbol{\theta}}]_{ij} \right\|_2 |[\mathbf{a}_{\boldsymbol{\theta}}]_i [\mathbf{a}_{\boldsymbol{\theta}}]_j| \leq \frac{N^{\frac{7}{2}} \sqrt{p} M_1^2 M_2}{\sigma_n^4}$$

2. The second and the third terms are identical with respect to bounding strategy:

$$\begin{aligned} \sum_{i=1}^N \sum_{j=1}^N \|\nabla_{\boldsymbol{\theta}} [[\mathbf{a}_{\boldsymbol{\theta}}]_i]\|_2 \left| [\mathbf{a}_{\boldsymbol{\theta}}]_j [\mathbf{B}_{\boldsymbol{\theta}}]_{ij} \right| &= \sum_{i=1}^N |\mathbf{B}_{\boldsymbol{\theta}}(i, \cdot) \mathbf{a}_{\boldsymbol{\theta}}| \|\nabla_{\boldsymbol{\theta}} [[\mathbf{a}_{\boldsymbol{\theta}}]_i]\|_2 \leq \\ \sum_{i=1}^N \|\mathbf{B}_{\boldsymbol{\theta}}(i, \cdot)\|_2 \|\mathbf{a}_{\boldsymbol{\theta}}\|_2 \|\nabla_{\boldsymbol{\theta}} [[\mathbf{a}_{\boldsymbol{\theta}}]_i]\|_2 &\leq \|\mathbf{B}_{\boldsymbol{\theta}}\|_F \|\mathbf{a}_{\boldsymbol{\theta}}\|_2 \sum_{i=1}^N \|\nabla_{\boldsymbol{\theta}} [[\mathbf{a}_{\boldsymbol{\theta}}]_i]\|_2 \end{aligned}$$

Since  $\|\mathbf{B}_{\boldsymbol{\theta}}\|_F \leq \sqrt{\text{rank}(\mathbf{B}_{\boldsymbol{\theta}})} \|\mathbf{B}_{\boldsymbol{\theta}}\|_2 \leq \frac{\sqrt{N}}{\sigma_n^2}$ . Hence,

$$\sum_{i=1}^N \sum_{j=1}^N \|\nabla_{\boldsymbol{\theta}} [[\mathbf{a}_{\boldsymbol{\theta}}]_i]\|_2 \left| [\mathbf{a}_{\boldsymbol{\theta}}]_j [\mathbf{B}_{\boldsymbol{\theta}}]_{ij} \right| \leq \frac{N\sqrt{N}M_1M_2}{\sigma_n^2}$$

Combining these results and using  $\|\nabla_{\boldsymbol{\theta}} k_{\boldsymbol{\theta}}(\mathbf{x}, \mathbf{x})\| \leq M_2$ ,  $|\sigma_{\boldsymbol{\theta}}(\mathbf{x}|\mathcal{D})| \geq k_{\boldsymbol{\theta}}(\mathbf{x}, \mathbf{x}) \geq M_0$ , we have:

$$\|\nabla_{\boldsymbol{\theta}} [\sigma_{\boldsymbol{\theta}}(\mathbf{x}|\mathcal{D})]\|_2 \leq \frac{N\sqrt{N}M_1M_2}{2\sigma_n^2M_0} \left[ \frac{N^2\sqrt{p}M_1}{\sigma_n^2} + 2 \right] \quad (13)$$

Hence, combining (12) and (13) we have:

$$\begin{aligned} \|\mathbf{h}_{\boldsymbol{\theta}}(\mathbf{x}|\mathcal{D})\|_2 &\leq \|\nabla_{\boldsymbol{\theta}} \mu_{\boldsymbol{\theta}}(\mathbf{x}|\mathcal{D})\|_2 + \sqrt{\frac{\beta\pi}{2}} \|\nabla_{\boldsymbol{\theta}} [\sigma_{\boldsymbol{\theta}}(\mathbf{x}|\mathcal{D})]\|_2 \leq \\ \frac{(C + M_4)N^2M_2}{\sigma_n^2} \left[ 1 + \frac{N^2M_1\sqrt{p}}{\sigma_n^2} \right] &+ \sqrt{\frac{\beta\pi}{2}} \frac{N\sqrt{N}M_1M_2}{2\sigma_n^2M_0} \left[ \frac{N^2\sqrt{p}M_1}{\sigma_n^2} + 2 \right] \triangleq A_1. \end{aligned}$$

Now, we are ready to bound the other two terms in the claim:

$$\mu_{\boldsymbol{\theta}+\epsilon}^2(\mathbf{x}|\mathcal{D}) \leq 2 [\mathbf{a}_{\boldsymbol{\theta}+\epsilon}^{\top} \mathbf{B}_{\boldsymbol{\theta}+\epsilon} (\mathbf{y} - \mathbf{m}_{\mathcal{D}})]^2 + 2|m|^2 \leq 2 \frac{(C + M_4)^2 M_1^2}{\sigma_n^4} + 2M_4^2$$

Therefore, for  $\mathbb{E}_{\epsilon} [\mu_{\boldsymbol{\theta}+\epsilon}^2(\mathbf{x}|\mathcal{D})]$  we have:

$$\mathbb{E}_{\epsilon} [\mu_{\boldsymbol{\theta}+\epsilon}^2(\mathbf{x}|\mathcal{D})] \leq 2 \frac{(C + M_4)^2 M_1^2}{\sigma_n^4} + 2M_4^2 \triangleq A_2.$$

Finally, for the posterior mean:

$$\sigma_{\theta+\epsilon}^2(\mathbf{x}|\mathcal{D}) \leq k_{\theta}(\mathbf{x}, \mathbf{x}) + \mathbf{a}_{\theta+\epsilon}^{\top} \mathbf{B}_{\theta+\epsilon} \mathbf{a}_{\theta+\epsilon} \leq M_1 + \frac{M_1^2}{\sigma_n^2}$$

Therefore, for  $\mathbb{E}_{\epsilon} [\sigma_{\theta+\epsilon}^2(\mathbf{x}|\mathcal{D})]$  we have:

$$\mathbb{E}_{\epsilon} [\sigma_{\theta+\epsilon}^2(\mathbf{x}|\mathcal{D})] \leq M_1 + \frac{M_1^2}{\sigma_n^2} \triangleq A_3.$$

This finishes the proof of the claim.  $\square$

Having equipped with these results, we can further simplify the setup expressions (6):

$$\sigma_n = \frac{\rho}{4\Phi^{-1}\left(1 - \frac{\delta}{8N_{\epsilon}}\right)}, \quad \sigma_{\epsilon} = \min \left\{ 1, \frac{\rho}{8 \left[ 2\sqrt{p} + \sqrt{\log \frac{4N_{\epsilon}}{\delta}} \right] [A_1 + o(1)]} \right\},$$

with

$$N_{\epsilon} = \left\lceil \frac{16 \left[ A_2 + \frac{\beta\pi}{2} A_3 \right]}{\delta\rho^2} \right\rceil.$$

This finishes the proof of the lemma.  $\square$

## C Experimental Details

### C.1 Black-Box Functions

As specified in Section 3, we evaluate black-box optimisation solvers based on their performances on a large set of tasks from Bayesmark package. Each task consists in optimising the hyper-parameters of a model to minimise the cross validation loss incurred when this model is applied to perform a regression (reg) or a classification (clf) on a given dataset. Thus, a task is characterised by a model, a dataset and a loss function, or metric, measuring the quality of the regression or classification. In total, 108 distinct tasks can be defined from the valid combination of the nine models specified in Table 2, the following six real-world UCI datasets [17], Boston (reg), Breast Cancer (clf), Diabetes (reg), Digits (clf), Iris (clf) and Wine (clf); the following two regression metrics, negative mean-squared error (MSE), negative mean absolute error (MAE), and two classification metrics, negative log-likelihood (NLL) and negative accuracy (ACC). The results reported in Figures 3 and 4 of the main paper have been obtained by applying each black-box optimisation method using 16 iterations of 8-batch acquisition steps on all of the 108 tasks. In order to provide a reliable evaluation of the different solvers, we repeated each run with 20 random seeds and considered the normalised score given by:

$$\text{Normalised Score} = 100 \times \frac{\mathcal{L} - \mathcal{L}^*}{\mathcal{L}^{\text{rand}} - \mathcal{L}^*} \quad (14)$$

where  $\mathcal{L}$  is the best-achieved cross validation loss at the end of the 16 acquisition steps,  $\mathcal{L}^*$  is the estimated optimal loss for the task and  $\mathcal{L}^{\text{rand}}$  is the mean loss (across multiple runs) obtained using random search with the same number of acquisition steps. The normalisation procedure allows to aggregate the scores across tasks although different cross-validation loss functions were used.

### C.2 Black-Box Optimisation Variables

We provide in Table 2 and Table 3 the list of the hyperparameters controlling the behaviour of each model along with their optimisation domains, which can differ whether the model is used for a classification or a regression task. The search domain can include a mix of continuous and integer variables (e.g. MLP-SGD set of hyperparameters includes a hidden layer size, which needs to be an integer, and an initial learning rate that can take any values between  $10^{-5}$  and  $10^{-1}$ ), and its dimensionality - which corresponds to the number of hyperparameters to tune - ranges from 2 to 9. We also specify in the last column of these Tables whether the search domain is modified through a standard transformation (log or logit) to ease optimisation.

Table 2: Search spaces for hyperparameter tuning on classification tasks. We specify the type of each hyperparameters (with  $\mathbb{R}$  for real-valued and  $\mathbb{Z}$  for integer valued) as well as the search domain. We specify  $\log -\mathcal{U}$  (resp.  $\text{logit} -\mathcal{U}$ ) to indicate that a log (resp. logit) transformation is applied to the optimisation domain.

Model	Parameter	Type	Domain
<b>kNN</b>	n_neighbors	$\mathbb{Z}$	$\mathcal{U}(1, 25)$
	p	$\mathbb{Z}$	$\mathcal{U}(1, 4)$
<b>Support Vector Machine</b>	C	$\mathbb{R}$	$\log -\mathcal{U}(1, 10^3)$
	gamma	$\mathbb{R}$	$\log -\mathcal{U}(10^{-4}, 10^{-3})$
	tol	$\mathbb{R}$	$\log -\mathcal{U}(10^{-5}, 10^{-1})$
	max_depth	$\mathbb{Z}$	$\mathcal{U}(1, 15)$
<b>Decision Tree</b>	min_samples_split	$\mathbb{R}$	$\text{logit} -\mathcal{U}(0.01, 0.99)$
	min_samples_leaf	$\mathbb{R}$	$\text{logit} -\mathcal{U}(0.01, 0.49)$
	min_weight_fraction_leaf	$\mathbb{R}$	$\text{logit} -\mathcal{U}(0.01, 0.49)$
	max_features	$\mathbb{R}$	$\text{logit} -\mathcal{U}(0.01, 0.99)$
	min_impurity_decrease	$\mathbb{R}$	$\mathcal{U}(0, 0.5)$
	max_depth	$\mathbb{Z}$	$\mathcal{U}(1, 15)$
<b>Random Forest</b>	max_features	$\mathbb{R}$	$\text{logit} -\mathcal{U}(0.01, 0.99)$
	min_samples_split	$\mathbb{R}$	$\text{logit} -\mathcal{U}(0.01, 0.99)$
	min_samples_leaf	$\mathbb{R}$	$\text{logit} -\mathcal{U}(0.01, 0.49)$
	min_weight_fraction_leaf	$\mathbb{R}$	$\text{logit} -\mathcal{U}(0.01, 0.49)$
	min_impurity_decrease	$\mathbb{R}$	$\mathcal{U}(0, 0.5)$
	hidden_layer_sizes	$\mathbb{Z}$	$\mathcal{U}(50, 200)$
<b>MLP-Adam</b>	alpha	$\mathbb{R}$	$\log -\mathcal{U}(10^{-5}, 10^1)$
	batch_size	$\mathbb{Z}$	$\mathcal{U}(10, 250)$
	learning_rate_init	$\mathbb{R}$	$\log -\mathcal{U}(10^{-5}, 10^{-1})$
	tol	$\mathbb{R}$	$\log -\mathcal{U}(10^{-5}, 10^{-1})$
	validation_fraction	$\mathbb{R}$	$\text{logit} -\mathcal{U}(0.1, 0.9)$
	beta_1	$\mathbb{R}$	$\text{logit} -\mathcal{U}(0.5, 0.99)$
	beta_2	$\mathbb{R}$	$\text{logit} -\mathcal{U}(0.9, 1 - 10^{-6})$
	epsilon	$\mathbb{R}$	$\log -\mathcal{U}(10^{-9}, 10^{-6})$
	hidden_layer_sizes	$\mathbb{Z}$	$\mathcal{U}(50, 200)$
	alpha	$\mathbb{R}$	$\log -\mathcal{U}(10^{-5}, 10^1)$
<b>MLP-SGD</b>	batch_size	$\mathbb{Z}$	$\mathcal{U}(10, 250)$
	learning_rate_init	$\mathbb{R}$	$\log -\mathcal{U}(10^{-5}, 10^{-1})$
	power_t	$\mathbb{R}$	$\text{logit} -\mathcal{U}(0.1, 0.9)$
	tol	$\mathbb{R}$	$\log -\mathcal{U}(10^{-5}, 10^{-1})$
	momentum	$\mathbb{R}$	$\text{logit} -\mathcal{U}(0.001, 0.999)$
	validation_fraction	$\mathbb{R}$	$\text{logit} -\mathcal{U}(0.1, 0.9)$
	n_estimators	$\mathbb{Z}$	$\mathcal{U}(10, 100)$
	learning_rate	$\mathbb{R}$	$\log -\mathcal{U}(10^{-4}, 10^1)$
	C	$\mathbb{R}$	$\log -\mathcal{U}(10^{-2}, 10^2)$
	intercept_scaling	$\mathbb{R}$	$\log -\mathcal{U}(10^{-2}, 10^2)$
<b>Linear</b>	C	$\mathbb{R}$	$\log -\mathcal{U}(10^{-2}, 10^2)$
	intercept_scaling	$\mathbb{R}$	$\log -\mathcal{U}(10^{-2}, 10^2)$



Table 3: Models and search spaces for hyperparameter tuning on regression tasks. Models having same search spaces for classification and regression tasks are omitted (see Table 2).

Model	Parameter	Type	Domain
<b>AdaBoost</b>	n_estimators	$\mathbb{Z}$	$\mathcal{U}(10, 100)$
	learning_rate	$\mathbb{R}$	$\log -\mathcal{U}(10^{-4}, 10^1)$
<b>Lasso</b>	alpha	$\mathbb{R}$	$\log -\mathcal{U}(10^{-2}, 10^2)$
	fit_intercept	$\mathbb{Z}$	$\mathcal{U}(0, 1)$
	normalize	$\mathbb{Z}$	$\mathcal{U}(0, 1)$
	max_iter	$\mathbb{Z}$	$\log -\mathcal{U}(10, 5000)$
	tol	$\mathbb{R}$	$\log -\mathcal{U}(10^{-5}, 10^{-1})$
	positive	$\mathbb{Z}$	$\mathcal{U}(0, 1)$
<b>Linear</b>	alpha	$\mathbb{R}$	$\log -\mathcal{U}(10^{-2}, 10^2)$
	fit_intercept	$\mathbb{Z}$	$\mathcal{U}(0, 1)$
	normalize	$\mathbb{Z}$	$\mathcal{U}(0, 1)$
	max_iter	$\mathbb{Z}$	$\log -\mathcal{U}(10, 5000)$
	tol	$\mathbb{R}$	$\log -\mathcal{U}(10^{-4}, 10^{-1})$

Algorithm	Mean	Std	Median	40 <sup>th</sup> Centile	30 <sup>th</sup> Centile	20 <sup>th</sup> Centile	5 <sup>th</sup> Centile
G-B0	<b>100.12</b>	<b>8.70</b>	<b>100.01</b>	<b>100.00</b>	<b>99.88</b>	<b>98.64</b>	<b>85.71</b>
PyS0t	98.18	9.03	100.00	99.81	98.60	95.36	80.00
TuRBO	97.95	10.80	100.00	99.88	98.75	95.26	78.63
HyperOpt	96.37	8.79	99.31	98.16	95.94	92.38	78.52
SkOpt	96.18	11.51	99.78	98.66	96.73	91.62	74.77
TuRBO+	95.29	10.93	98.97	97.60	95.27	90.92	74.77
OpenTuner	94.32	14.18	98.44	96.93	93.84	89.97	68.96
NeverGrad	93.20	17.52	99.65	97.84	94.57	88.28	55.34
BOHB	92.03	11.16	96.02	93.55	90.14	85.71	67.82
Random-Search	92.00	11.71	96.18	93.55	90.05	85.16	69.55

Table 4: Mean and n-th percentile normalized scores over 108 black-box functions, each repeated with 20 random seeds. We see significant mean improvements from G-B0 compared with all other algorithms.

### C.3 Additional Results

Table 4 synthesises the performances achieved on the 108 tasks by the black-box optimisation solvers considered in our experiments. We note that the distribution of the scores attained by G-B0 has the largest mean and the smallest standard-deviation, indicating significant out-performance of this method over alternative solvers. In a complementary fashion, normalised score distributions obtained on each task by each black-box optimisers are provided in Figure 5. Each dataset, model pair have two available metrics for each classification/ regression scenario. In order for easier visualisation we reduce the tasks from 108 to 52 by averaging each seed over the normalised score achieved for both metrics (MAE, MSE) for regression and (NLL, ACC) for classification tasks. In summary, we see G-B0 outperforming all other baselines in 32 out of 54 tasks (59%).

### C.4 Implementation Details for BOHB

BOHB is a scalable hyper-parameter tuning algorithm introduced in [8] mixing bandits and BO approaches to achieve strong anytime and final performances. Contrary to the other solvers considered in this paper, BOHB is specifically designed to tackle multi-fidelity optimisation and it uses Hyperband [9] routine to define the fidelity levels under which points are asynchronously evaluated. The selection of points follows a BO strategy based on Tree Parzen Estimator (TPE) method. Given a dataset  $\mathcal{D}$  of already observed data points and a threshold  $\alpha \in \mathbb{R}$ , the TPE models  $p(\mathbf{x}|y)$  using

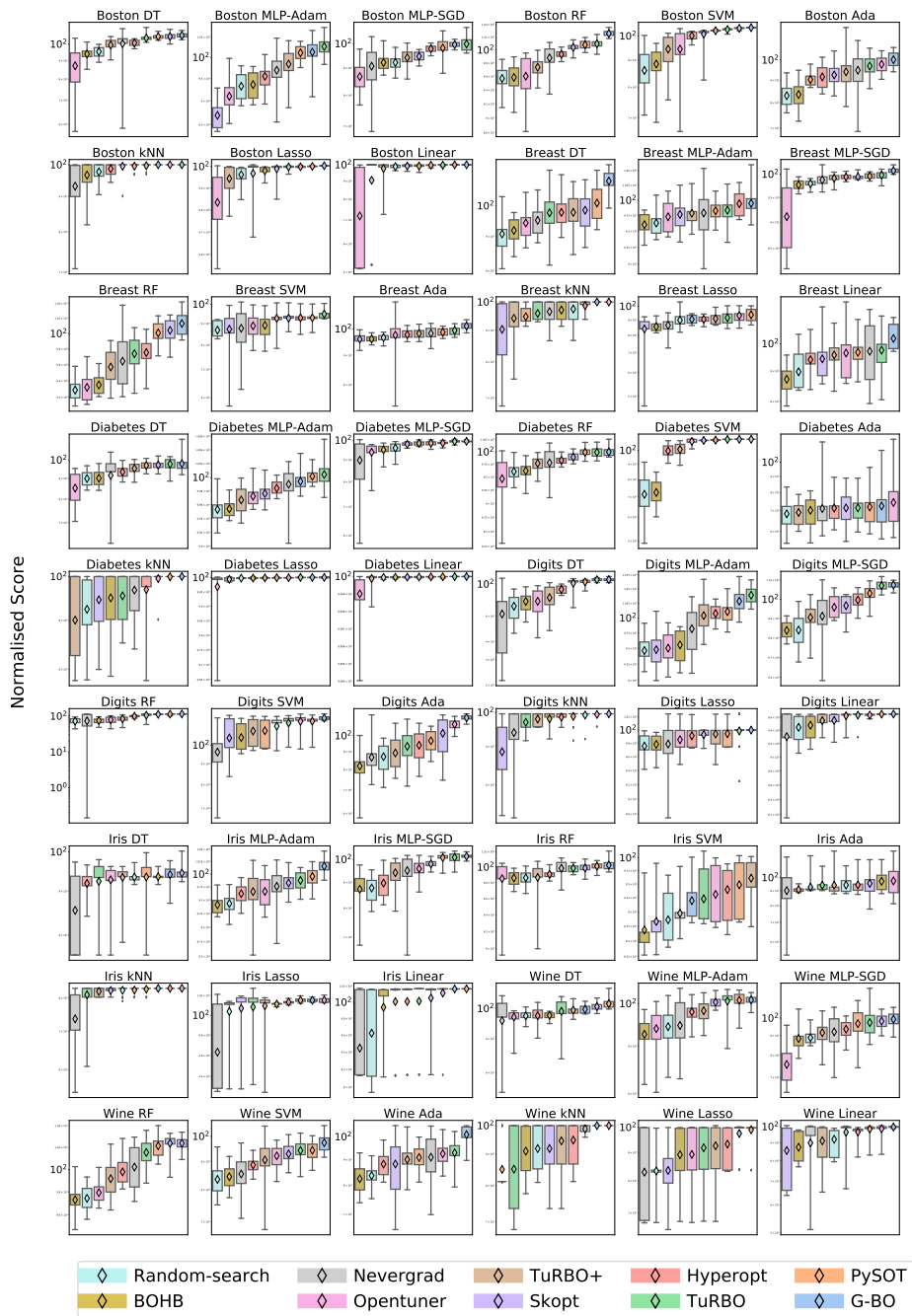


Figure 5: Normalised score (see 14) obtained by each black-box optimiser on all tasks. On each graph optimisers are ranked by mean scores. Overall we see G-BO outperforming all other baselines in 32 out of 54 tasks (59%).

kernel density estimations of

$$\begin{aligned}\ell(\mathbf{x}) &= p(y < \alpha | \mathbf{x}, \mathcal{D}) \\ g(\mathbf{x}) &= p(y \geq \alpha | \mathbf{x}, \mathcal{D}).\end{aligned}$$

In the TPE algorithm, maximising the expected improvement criterion

$$\alpha_{\text{EI}}(\mathbf{x}) = \int \max(0, \alpha - p(y | \mathbf{x})) p(y | \mathbf{x}) dy$$

is equivalent to maximising the ratio  $r(\mathbf{x}) = \frac{\ell(\mathbf{x})}{g(\mathbf{x})}$  which is carried out to select a single new candidate point at a time.

In the absence of a multi-fidelity setup in our experiments, we ran a modified version of the BOHB algorithm implemented in the HpBandSter package. We left the TPE method for modelling unchanged but we ignored the fidelity level assignment from Hyperband. Moreover, as our experimental setup involves batch-acquisitions, we tested two alternatives to the standard BOHB acquisition procedure to support synchronous suggestion of multiple points. In a first approach, we run  $q$  independent maximisation processes of  $r(\mathbf{x})$  from random starting points and recover a single candidate from each process to form the  $q$ -batch suggestion. In a second approach, we obtain one point as a result of a single maximisation of  $r(\mathbf{x})$  and we sample  $q - 1$  random points to complete the  $q$ -batch suggestion. As the latter method yields better overall performance, the results reported in this work under BOHB label have been obtained using the second approach.

## D Hypothesis Testing for Heteroscedasticity

GP modelling usually considers a conditional normal distribution of the observations  $y | \cdot \sim \mathcal{N}(f(\cdot), \sigma^2(\cdot))$ . In most cases GP regression is run assuming  $\sigma(\cdot)^2$  to be constant, in which case the GP is called homoscedastic. To assess whether this assumption holds for the tasks under examination, we used Levine’s test and the Fligner and Killeen test.

To run these tests on a given task, we evaluated  $k = 50$  distinct sets of hyperparameters  $\{x_i\}_{1 \leq i \leq k}$  for  $n = 10$  times and obtained scores  $\{Y_{ij}\}_{1 \leq i \leq k, 1 \leq j \leq n}$ , where  $Y_{ij}$  is the  $j^{\text{th}}$  score observed when evaluating the  $i^{\text{th}}$  configuration. For  $i = 1, \dots, k$ , let  $\sigma_i^2$  denote the observed variance of  $y | x_i$ , then both Levine’s and Fligner and Killeen tests share the same null hypothesis of homoscedasticity:

$$H_0 : \sigma_1^2 = \dots = \sigma_k^2.$$

In all 108 tests, we see a p-value significantly lower than 0.05 in 72 tasks using Levine’s test, and in 73 tasks using Fligner and Killeen. Such results (shown in detail in Appendix D) imply that at least 66% of the experimental tasks exhibit heteroscedastic behaviour. Additionally, Figure 6 illustrates the heteroscedasticity of several tasks showing drastic changes of the observed noise level around the mean validation accuracy (**hyper-parameter** <sub>$i$</sub> ) for varying values of hyper-parameter.

### D.1 Levine’s Test

Levine’s test statistic is defined as

$$W = \frac{N - k}{k - 1} \cdot \frac{\sum_{i=1}^k n(\bar{Z}_i - \bar{Z}_{..})^2}{\sum_{i=1}^k \sum_{j=1}^n (Z_{ij} - \bar{Z}_i)^2}$$

where  $N = k \times n$ ,  $Z_{ij} = |Y_{ij} - \frac{1}{n} \sum_{j=1}^n Y_{ij}|$ ,  $\bar{Z}_i = \frac{1}{n} \sum_{j=1}^n Z_{ij}$  and  $\bar{Z}_{..} = \frac{1}{k} \sum_{i=1}^k \bar{Z}_i$ , for all  $i = 1, \dots, k$ ,  $j = 1, \dots, n$ . The Levine test rejects the homoscedasticity hypothesis  $H_0$  if

$$W > F_{\alpha, k-1, N-k}$$

where  $F_{\alpha, k-1, N-k}$  is the upper critical value at a significance level  $\alpha$  of the  $F$  distribution with  $k - 1$  and  $N - k$  degrees of freedom.

Fligner and Killeen test is an alternative to Levine’s test that is particularly robust to outliers.

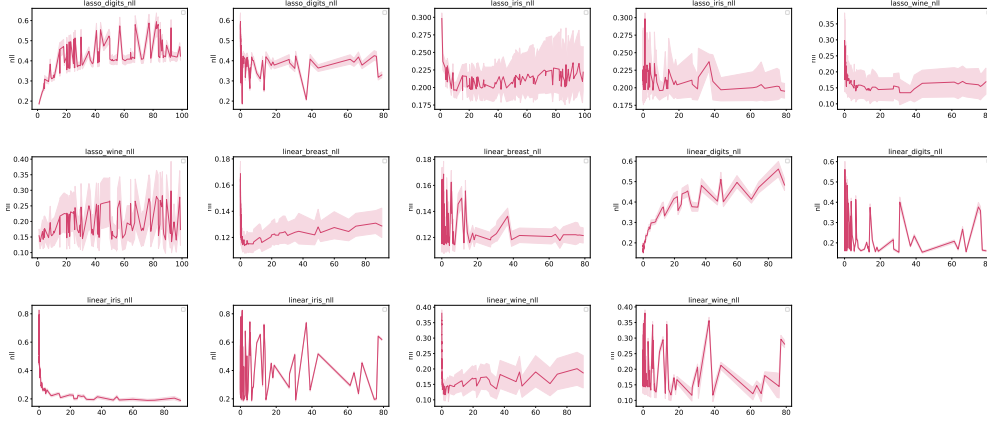


Figure 6: These figures show for several tasks the evolution of the observed noise level as hyperparameter values vary. Changes in the standard deviation magnitude (represented by the shaded areas) indicate that the noise level depends on the hyperparameter value, in other words they indicate heteroscedasticity. Drastic changes in standard deviation level are notably observed for (Lasso, Iris, NLL) or (Linear, Digits, NLL) tasks.

## D.2 Fligner & Killeen Test

Computation of the Fligner and Killeen test requires ranking all the absolute values  $\{|Y_{ij} - \tilde{Y}_i|\}_{1 \leq i \leq k, 1 \leq j \leq n}$  where  $\tilde{Y}_i$  is the median of  $\{Y_{ij}\}_{1 \leq j \leq n}$ . Increasing scores  $a_{N,r} = \Phi^{-1}\left(\frac{1 + \frac{r}{N+1}}{2}\right)$  are associated to each rank  $r = 1, \dots, N$ , where  $N = kn$  and  $\Phi(\cdot)$  is the cumulative distribution function for a standard normal variable. We denote the rank score associated to  $Y_{ij}$  as  $r_{ij}$ .

The Fligner and Killeen test statistic is given by

$$\chi_o^2 = \frac{\sum_{i=1}^k n (\bar{A}_i - \bar{a})^2}{V^2}$$

where  $\bar{A}_i = \frac{1}{n} \sum_{j=1}^n a_{N,r_{ij}}$ ,  $\bar{a} = \frac{1}{N} \sum_{r=1}^N a_{N,r}$  and  $V^2 = \frac{1}{N-1} \sum_{r=1}^N (a_{N,r} - \bar{a})^2$ .

As  $\chi_0$  has asymptotic  $\chi^2$  distribution with  $(k-1)$  degrees of freedom, therefore the test rejects the homoscedasticity hypothesis  $H_0$  if

$$\chi_0 > \chi_{\alpha, k-1}^2$$

where  $\chi_{\alpha, k-1}^2$  is the upper critical value at a significance level  $\alpha$  of the  $\chi^2$  distribution with  $k-1$  degrees of freedom.

The results of the Levine test as well as the Fligner and Killeen test are reported in Tables 5-10.

## E Acquisition Function Conflicts

The full set of experiments described in section 3.3 of the main paper, highlighting conflicts of widely used acquisition functions, can be visualised in Figures 7-12. For each plot, respective maximisers of EI, PI and UCB are shown with vertical lines to clearly indicate when optimising different acquisition functions leads to conflicting recommendations.

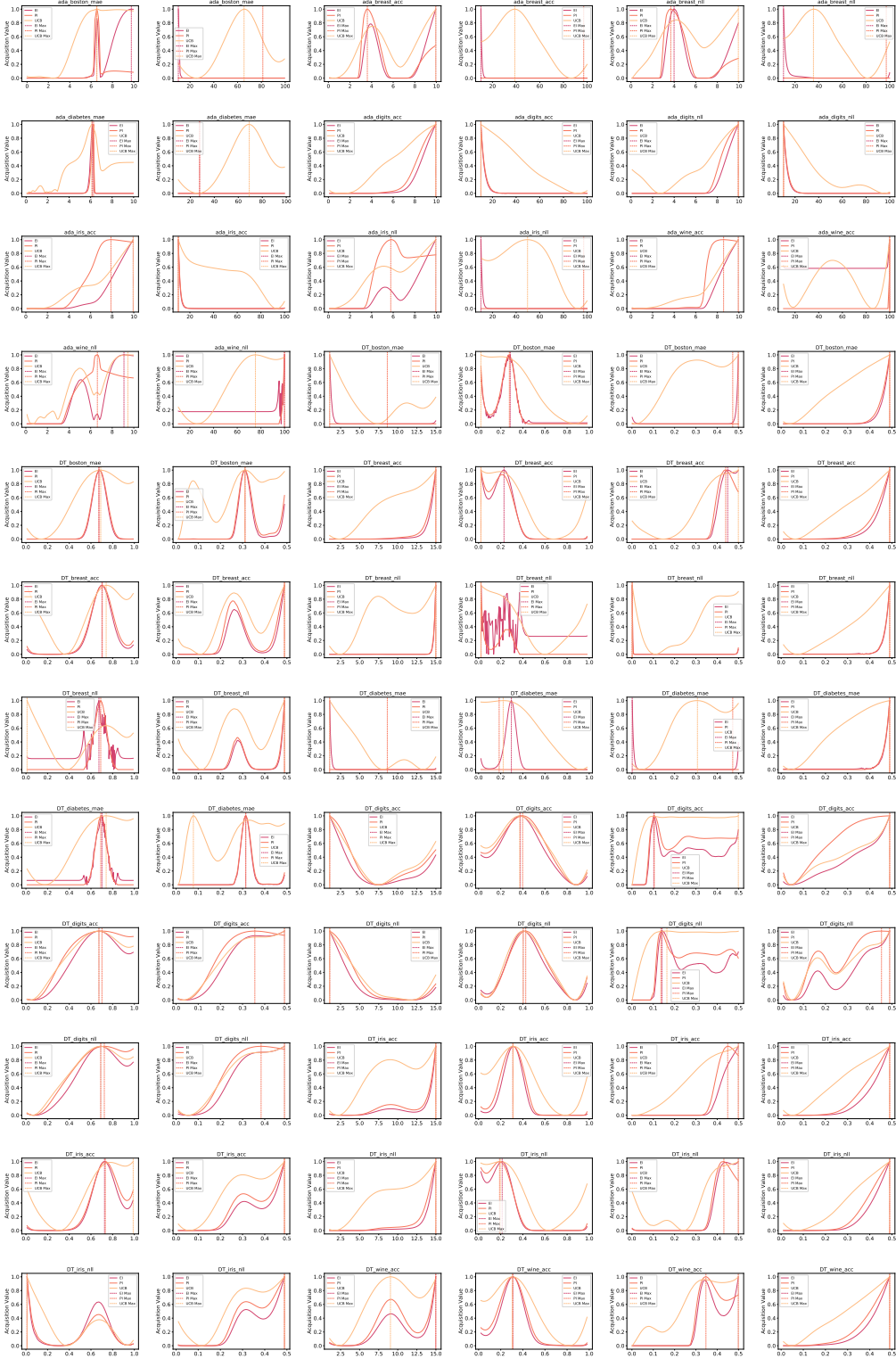


Figure 7: Conflicting acquisition functions

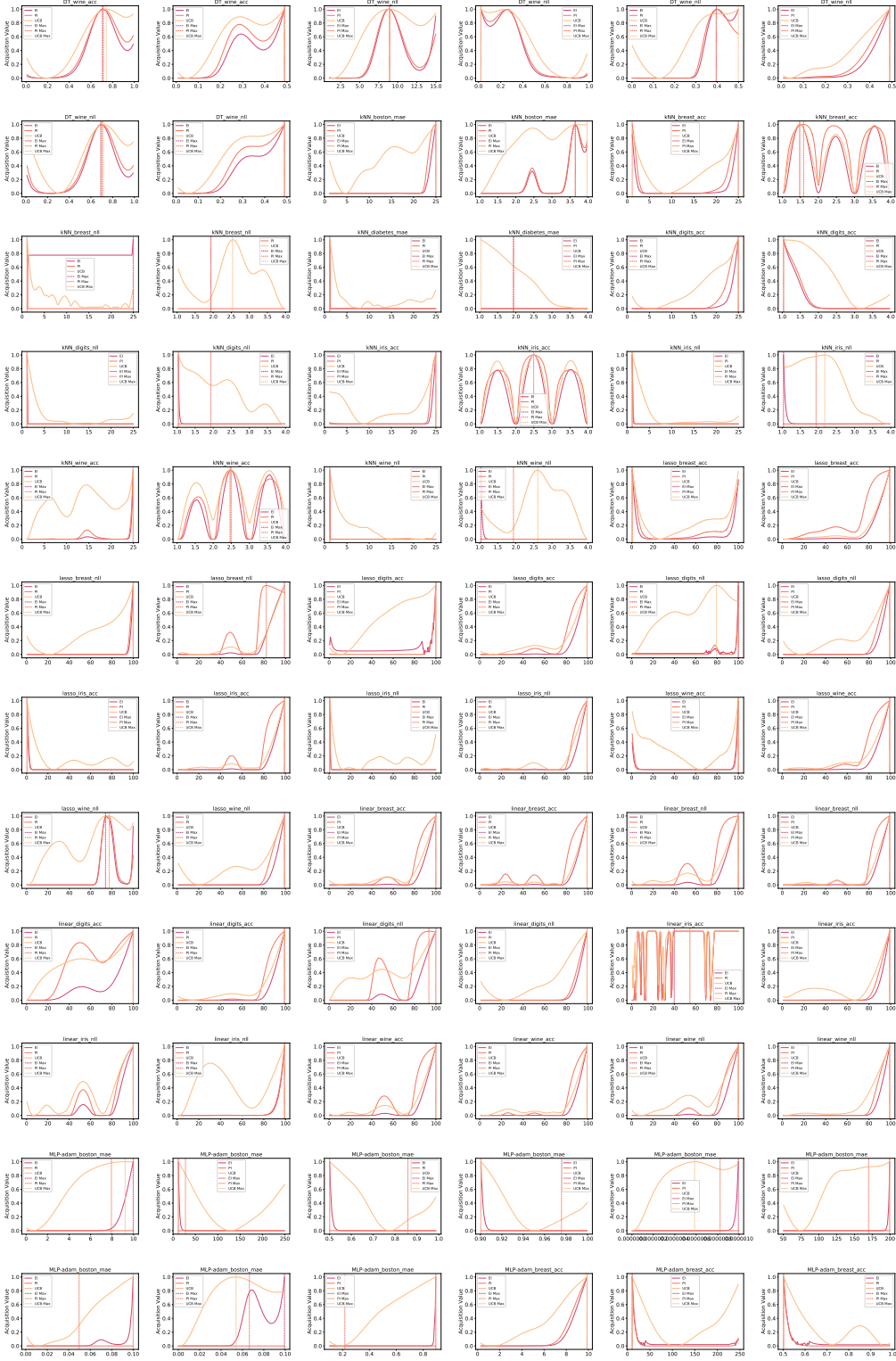


Figure 8: Conflicting acquisition functions

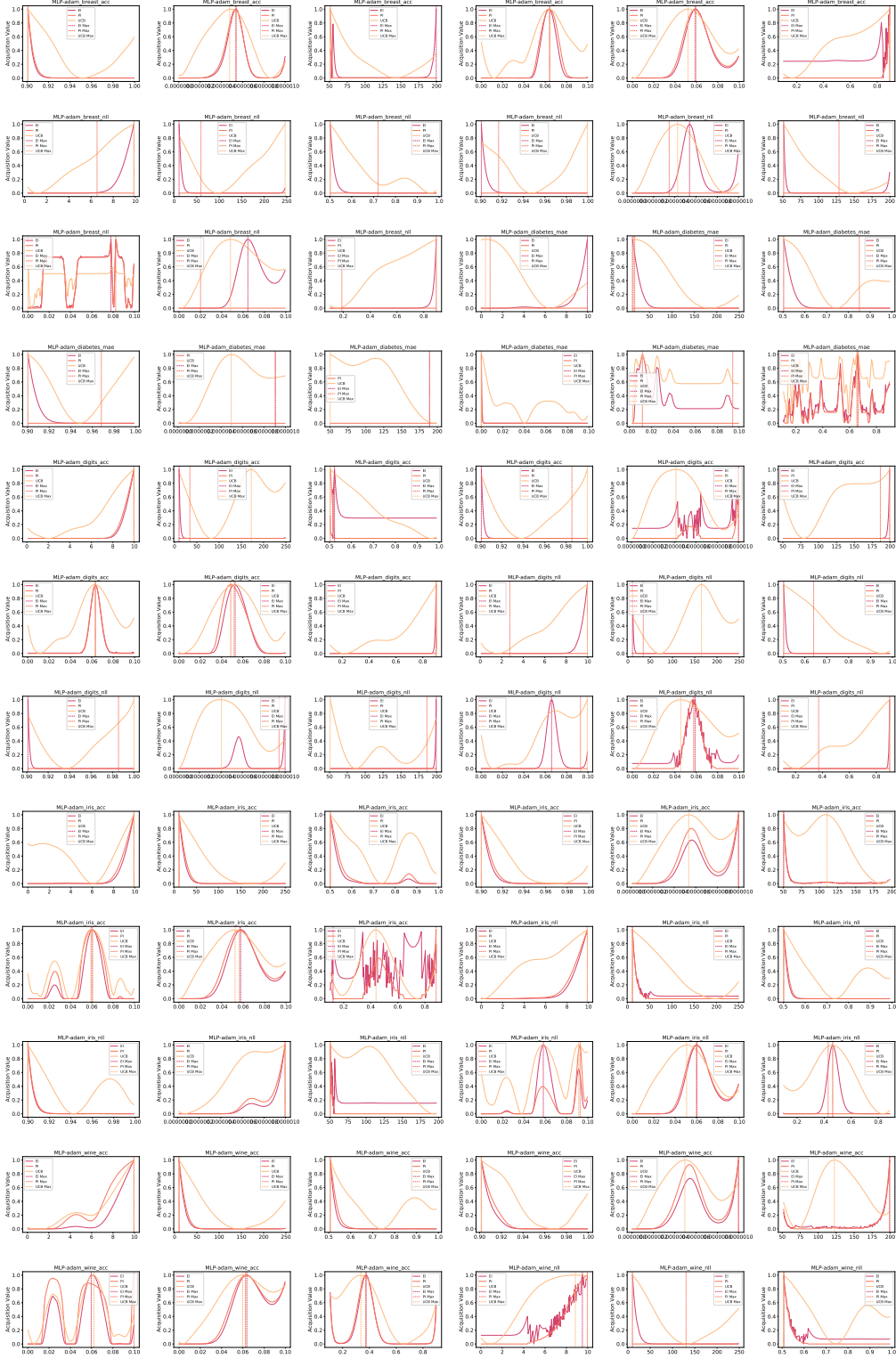


Figure 9: Conflicting acquisition functions

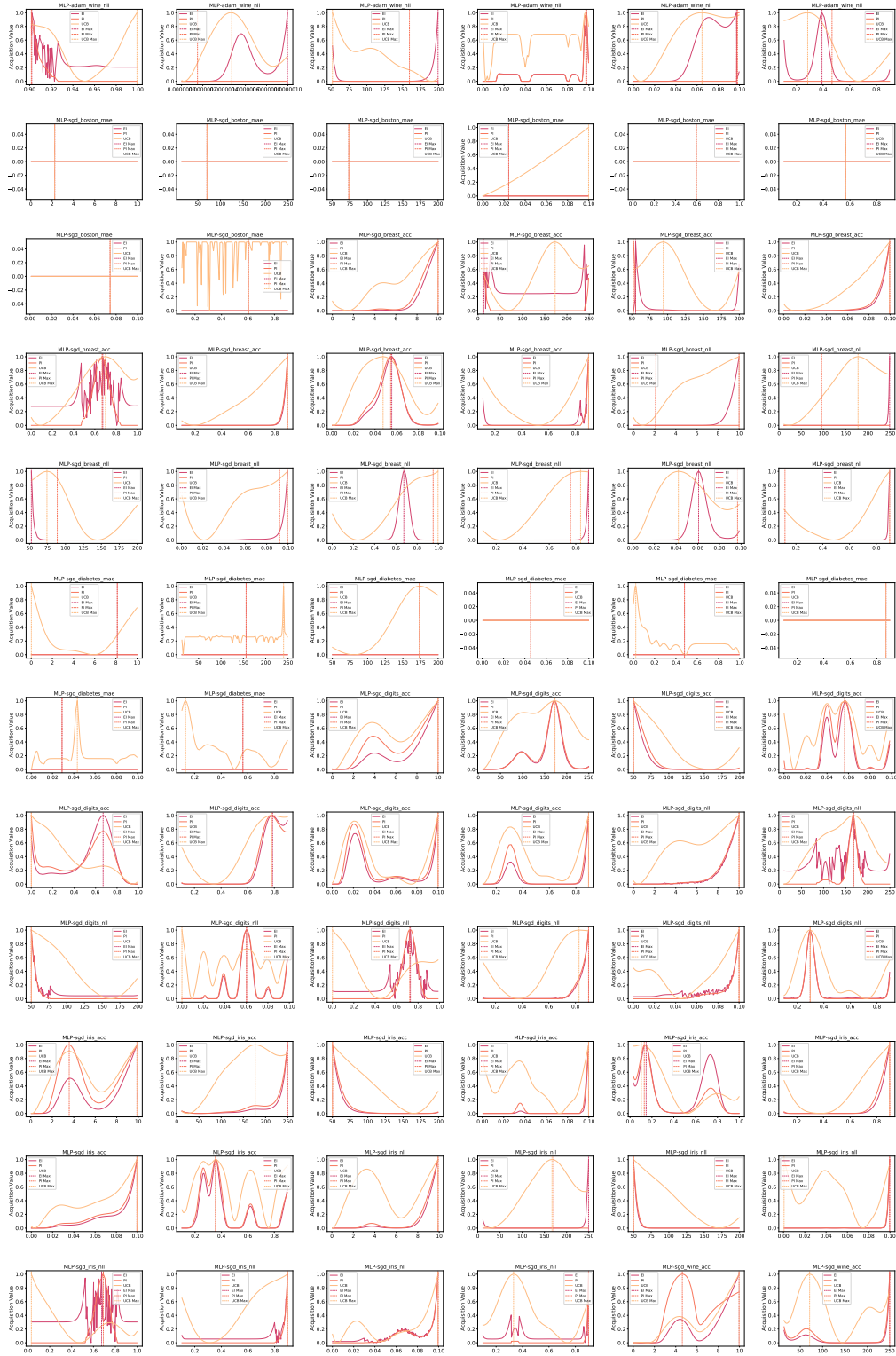


Figure 10: Conflicting acquisition functions



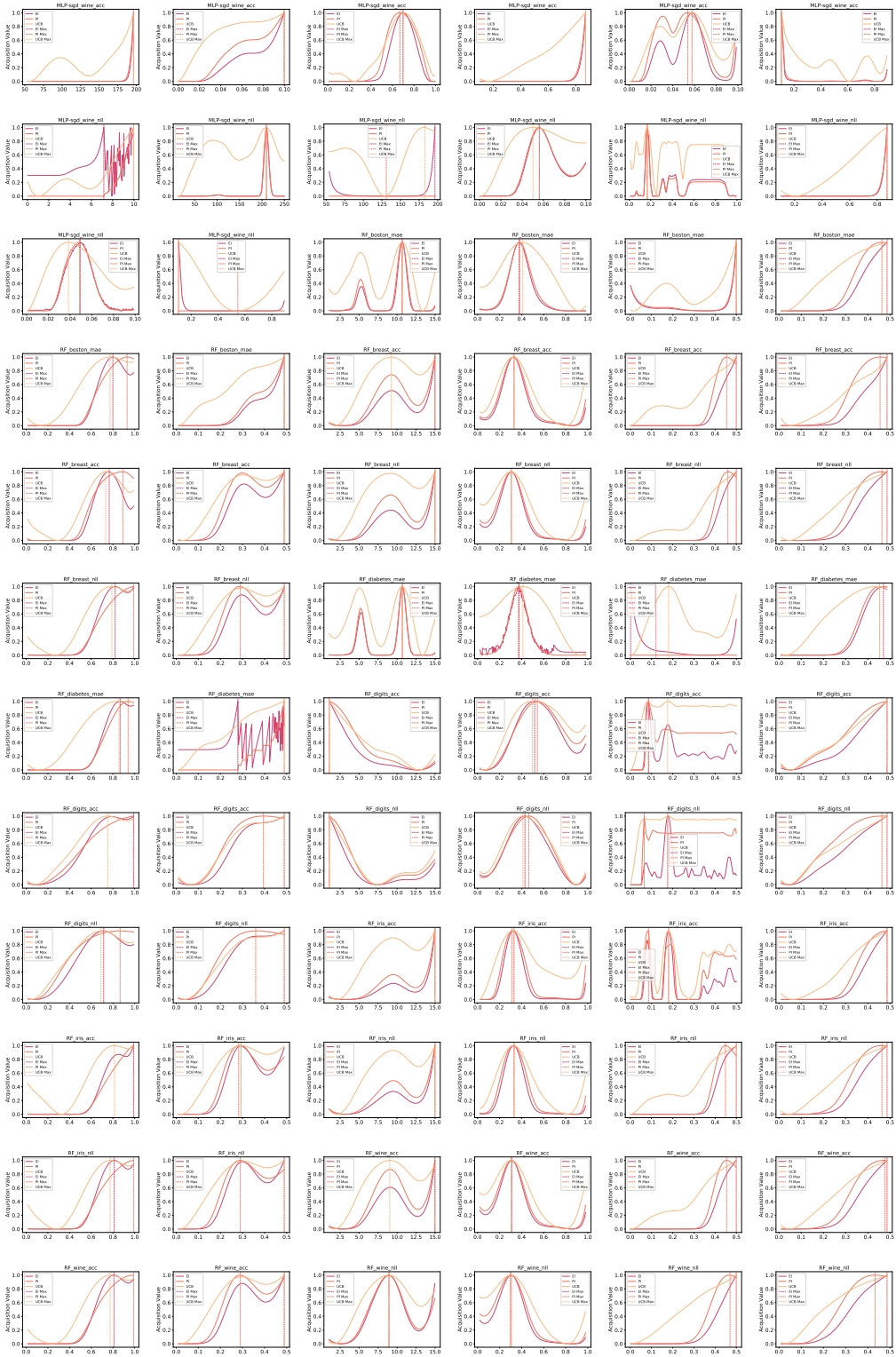


Figure 11: Conflicting acquisition functions

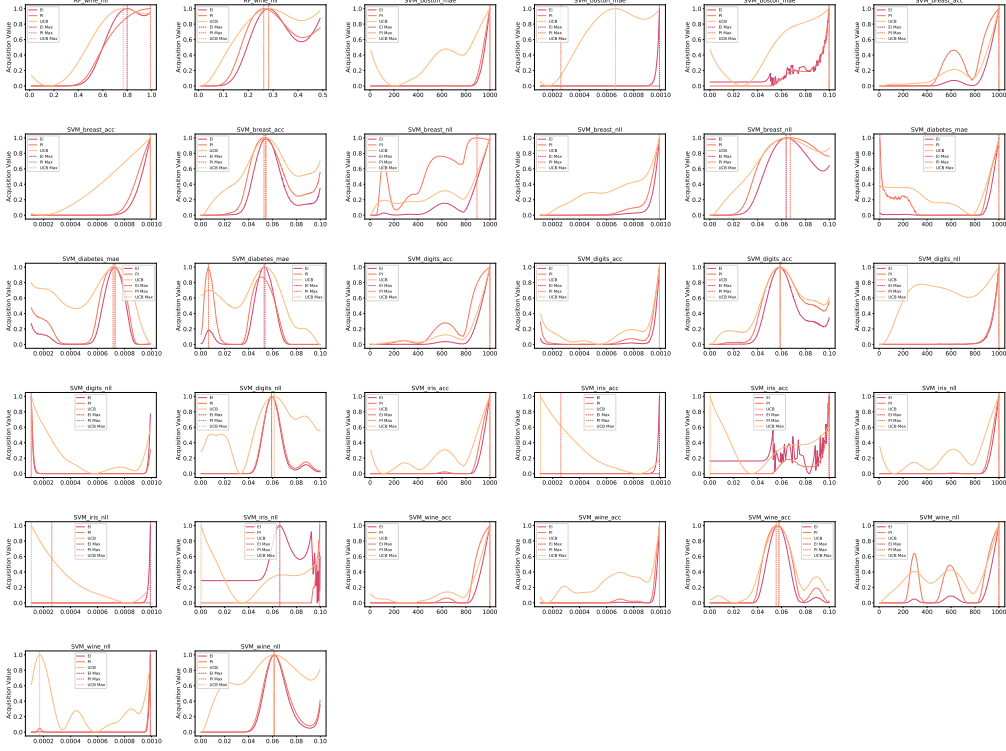


Figure 12: Conflicting acquisition functions

Table 5: Heteroscedasticity tests on tasks involving wine dataset

Dataset	Model	Metrics	Fligner Statistic	Fligner p-value	Levene Statistic	Levene p-value
wine	DT	acc	127.3	<b>6.912e-09</b>	3.553	<b>7.195e-13</b>
	MLP-adam	acc	85.37	<b>9.945e-04</b>	1.874	<b>5.544e-04</b>
	MLP-sgd	acc	109	<b>1.845e-06</b>	2.48	<b>5.701e-07</b>
	RF	acc	128.5	<b>4.717e-09</b>	5.069	<b>2.014e-21</b>
	SVM	acc	28.73	0.9908	0.5136	0.9975
	ada	acc	156.6	<b>3.527e-13</b>	3.968	<b>3.215e-15</b>
	kNN	acc	37.67	0.8807	0.6869	0.9473
	lasso	acc	29.8	0.9862	0.5981	0.9859
	linear	acc	21.28	0.9998	0.3839	1
	DT	nll	349.2	<b>6.614e-47</b>	10.46	<b>1.115e-48</b>
	MLP-adam	nll	57.19	0.1971	1.21	0.1646
	MLP-sgd	nll	110.1	<b>1.362e-06</b>	2.597	<b>1.380e-07</b>
	RF	nll	258	<b>3.660e-30</b>	6.468	<b>4.597e-29</b>
	SVM	nll	57.18	0.1975	1.006	0.4663
	ada	nll	152.8	<b>1.323e-12</b>	3.072	<b>3.555e-10</b>
	kNN	nll	178.2	<b>1.410e-16</b>	5.446	<b>1.635e-23</b>
	lasso	nll	83.94	<b>1.394e-03</b>	1.782	<b>1.416e-03</b>
	linear	nll	185.8	<b>8.404e-18</b>	5.01	<b>4.312e-21</b>

Table 6: Heteroscedasticity tests on tasks involving breast dataset

Dataset	Model	Metrics	Fligner Statistic	Fligner p-value	Levene Statistic	Levene p-value
<b>breast</b>	DT	acc	97.79	<b>4.302e-05</b>	4.62	<b>6.650e-19</b>
	MLP-adam	acc	133	<b>1.113e-09</b>	2.939	<b>1.923e-09</b>
	MLP-sgd	acc	116.8	<b>1.854e-07</b>	2.469	<b>6.495e-07</b>
	RF	acc	154.9	<b>6.469e-13</b>	6.661	<b>4.353e-30</b>
	SVM	acc	20.7	0.9999	0.3995	0.9999
	ada	acc	272.5	<b>9.178e-33</b>	13.57	<b>6.582e-62</b>
	kNN	acc	33.16	0.9596	0.5519	0.9941
	lasso	acc	20.78	0.9999	0.4291	0.9998
	linear	acc	21.15	0.9998	0.4545	0.9995
	DT	nll	260.5	<b>1.280e-30</b>	9.52	<b>2.294e-44</b>
	MLP-adam	nll	166.6	<b>1.008e-14</b>	3.643	<b>2.247e-13</b>
	MLP-sgd	nll	141.2	<b>7.115e-11</b>	2.669	<b>5.661e-08</b>
	RF	nll	185.8	<b>8.495e-18</b>	7.553	<b>1.013e-34</b>
	SVM	nll	76.98	<b>6.526e-03</b>	1.707	<b>2.970e-03</b>
	ada	nll	142	<b>5.458e-11</b>	4.283	<b>5.274e-17</b>
	kNN	nll	125.7	<b>1.155e-08</b>	4.337	<b>2.635e-17</b>
	lasso	nll	71.41	<b>0.02</b>	1.011	0.4565
	linear	nll	18.55	1	0.2714	1

Table 7: Heteroscedasticity tests on tasks involving boston dataset

Dataset	Model	Metrics	Fligner Statistic	Fligner p-value	Levene Statistic	Levene p-value
<b>boston</b>	DT	mae	73.51	<b>0.01327</b>	1.752	<b>1.900e-03</b>
	MLP-adam	mae	336.3	<b>1.737e-44</b>	14.4	<b>3.611e-65</b>
	MLP-sgd	mae	272.6	<b>8.694e-33</b>	6.561	<b>1.480e-29</b>
	RF	mae	28.79	0.9906	0.6768	0.9537
	SVM	mae	48.08	0.5106	0.9612	0.5508
	ada	mae	218.7	<b>2.692e-23</b>	13.59	<b>5.542e-62</b>
	kNN	mae	33.15	0.9597	0.619	0.98
	lasso	mae	30.4	0.983	0.6091	0.983
	linear	mae	16.17	1	0.251	1
	DT	mse	60.75	0.1211	1.33	0.07387
	MLP-adam	mse	387	<b>4.504e-54</b>	15.32	<b>1.147e-68</b>
	MLP-sgd	mse	353.2	<b>1.185e-47</b>	8.239	<b>3.548e-38</b>
	RF	mse	35.59	0.9242	0.8985	0.6692
	SVM	mse	25.01	0.9983	0.4491	0.9996
	ada	mse	249.1	<b>1.398e-28</b>	14.4	<b>3.682e-65</b>
	kNN	mse	27.75	0.9938	0.8247	0.7951
	lasso	mse	31.38	0.9764	0.5397	0.9955
	linear	mse	16.67	1	0.1726	1

Table 8: Heteroscedasticity tests on tasks involving diabetes dataset

Dataset	Model	Metrics	Fligner Statistic	Fligner p-value	Levene Statistic	Levene p-value
<b>diabetes</b>	DT	mae	56.52	0.2146	1.131	0.2601
	MLP-adam	mae	74.64	<b>0.01059</b>	2.573	<b>1.847e-07</b>
	MLP-sgd	mae	191.3	<b>1.062e-18</b>	17.87	<b>8.498e-78</b>
	RF	mae	79.38	<b>3.898e-03</b>	1.558	<b>0.01174</b>
	SVM	mae	2.436	1	1.810e-04	1
	ada	mae	179.8	<b>7.883e-17</b>	7.542	<b>1.154e-34</b>
	kNN	mae	67.48	<b>0.04106</b>	2.101	<b>4.747e-05</b>
	lasso	mae	176.2	<b>2.950e-16</b>	4.75	<b>1.225e-19</b>
	linear	mae	206	<b>3.792e-21</b>	5.714	<b>5.490e-25</b>
	DT	mse	44.52	0.6551	0.8264	0.7925
	MLP-adam	mse	100.4	<b>2.109e-05</b>	3.582	<b>4.951e-13</b>
	MLP-sgd	mse	202.9	<b>1.257e-20</b>	14.31	<b>7.960e-65</b>
	RF	mse	37.1	0.8938	0.8063	0.8224
	SVM	mse	4.004	1	4.740e-04	1
	ada	mse	189	<b>2.510e-18</b>	7.348	<b>1.138e-33</b>
	kNN	mse	88.62	<b>4.545e-04</b>	2.964	<b>1.407e-09</b>
	lasso	mse	257.6	<b>4.341e-30</b>	10.86	<b>1.637e-50</b>
	linear	mse	278.2	<b>8.540e-34</b>	10.01	<b>1.216e-46</b>

Table 9: Heteroscedasticity tests on tasks involving digits dataset

Dataset	Model	Metrics	Fligner Statistic	Fligner p-value	Levene Statistic	Levene p-value
<b>digits</b>	DT	acc	205	<b>5.670e-21</b>	14.29	<b>9.219e-65</b>
	MLP-adam	acc	256.7	<b>6.239e-30</b>	7.342	<b>1.219e-33</b>
	MLP-sgd	acc	210	<b>8.188e-22</b>	6.53	<b>2.167e-29</b>
	RF	acc	184.3	<b>1.458e-17</b>	15.61	<b>9.379e-70</b>
	SVM	acc	91.72	<b>2.093e-04</b>	2.187	<b>1.790e-05</b>
	ada	acc	99.34	<b>2.832e-05</b>	2.305	<b>4.601e-06</b>
	kNN	acc	35	0.9343	0.7042	0.9349
	lasso	acc	22.97	0.9994	0.4292	0.9998
	linear	acc	17.3	1	0.2963	1
	DT	nll	249.6	<b>1.140e-28</b>	15.71	<b>3.892e-70</b>
	MLP-adam	nll	339.8	<b>3.816e-45</b>	6.882	<b>3.012e-31</b>
	MLP-sgd	nll	244.8	<b>7.740e-28</b>	6.104	<b>4.129e-27</b>
	RF	nll	144	<b>2.791e-11</b>	7.435	<b>4.059e-34</b>
	SVM	nll	4.373	1	0.06091	1
	ada	nll	135.1	<b>5.444e-10</b>	3.294	<b>2.061e-11</b>
	kNN	nll	108.2	<b>2.326e-06</b>	3.059	<b>4.211e-10</b>
	lasso	nll	88.4	<b>4.799e-04</b>	2.116	<b>3.995e-05</b>
	linear	nll	103	<b>1.024e-05</b>	3.328	<b>1.335e-11</b>

Table 10: Heteroscedasticity tests on tasks involving iris dataset

Dataset	Model	Metrics	Fligner Statistic	Fligner p-value	Levene Statistic	Levene p-value
<b>iris</b>	DT	acc	207.1	<b>2.440e-21</b>	6.523	<b>2.355e-29</b>
	MLP-adam	acc	83.81	<b>1.436e-03</b>	1.838	<b>7.989e-04</b>
	MLP-sgd	acc	68.52	<b>0.03413</b>	1.409	<b>0.04082</b>
	RF	acc	155.5	<b>5.311e-13</b>	6.138	<b>2.726e-27</b>
	SVM	acc	198.4	<b>6.990e-20</b>	3.345	<b>1.065e-11</b>
	ada	acc	155.7	<b>4.788e-13</b>	5.018	<b>3.858e-21</b>
	kNN	acc	55.68	0.2378	1.124	0.2701
	lasso	acc	19.72	0.9999	0.4045	0.9999
	linear	acc	106.4	<b>3.965e-06</b>	2.959	<b>1.502e-09</b>
	DT	nll	322.2	<b>7.375e-42</b>	6.118	<b>3.506e-27</b>
	MLP-adam	nll	106.3	<b>4.070e-06</b>	3.123	<b>1.869e-10</b>
	MLP-sgd	nll	155.6	<b>4.966e-13</b>	6.386	<b>1.264e-28</b>
	RF	nll	321.3	<b>1.066e-41</b>	8.339	<b>1.136e-38</b>
	SVM	nll	188.4	<b>3.217e-18</b>	4.736	<b>1.470e-19</b>
	ada	nll	74.04	<b>0.01194</b>	1.414	<b>0.03938</b>
	kNN	nll	212.6	<b>2.863e-22</b>	8.838	<b>4.118e-41</b>
	lasso	nll	45.45	0.6177	0.5045	0.998
	linear	nll	36.64	0.9037	0.733	0.9101